A Precision Measurement of the Neutral Pion Lifetime via the Primakoff Effect

TJNAF PAC 15 Proposal

December 17, 1998

K. A. Assamagan, L. Gan, A. Gasparian (spokesperson and contact person),
W. Buck, J. Goity, P. Gueye, L. Tang, C. Keppel, K. Baker
Hampton University, Hampton, VA

B. Asavapibhop, R. Hicks, D. Lawrence, R. Miskimen (spokesperson), G. Peterson, J. Shaw
University of Massachusetts, Amherst, MA

A. Ahmidouch, S. Danagoulian (spokesperson), C. Jackson, S. Mtingwa, R. Sawafta
North Carolina A&T State University, Greensboro, NC

D. Dale (spokesperson), T. Gorringe, W. Korsch, C. Popescu,
V. Zeps, P. Zolnierczuk
University of Kentucky, Lexington, KY

E. Chudakoff, R. Ent, V. Gyurjyan, M. Ito, B. Wojtsekhowski
J.P. Chen, D. Mack, E. Smith
Thomas Jefferson National Accelerator Facility, Newport News, VA

A. Bernstein, M. Distler, M. Pavan
Massachusetts Institute of Technology, Cambridge, MA

A. Nathan
University of Illinois, Urbana, IL

D. Sober, H. Crannell, A. Longhi
The Catholic University of America, Washington, DC

W. Briscoe, L. Murphy
George Washington University, Washington, DC

I. Aznauryan, H. Egiyan, S. Gevorgyan, A. Margaryan, K. Egiyan, S. Stepanyan,
H. Voskanyan, A. Ketikyan, A. Shahinyan,Y. Sharabian, A. Petrosyan
Yerevan Physics Institute, Yerevan, Armenia

A. Glamazdin, A. Omelaenko
Kharkov Institute of Physics and Technology, Kharkov, Ukraine

A. Afanasev
North Carolina Central University, Durham, NC

B. Milbrath
Eastern Kentucky University, Richmond, KY

A.I. Fix, V.A. Tryasuchev
Tomsk Polytechnical University, Tomsk, Russia

Abstract

We propose to perform a precise measurement of the neutral pion lifetime using the small angle coherent photoproduction of π^o's in the Coulomb field of a nucleus, *i.e.* the Primakoff effect. The $\pi^o \to \gamma\gamma$ decay proceeds primarily via the chiral anomaly and represents one of the most definitive tests of low energy QCD. This measurement will be a state-of-the-art experimental determination of the lifetime with a precision of less than 1.5%, which is commensurate with the theoretical uncertainty. The π^o photoproduction cross section will be measured for three nuclei (^{12}C, ^{116}Sn, and ^{208}Pb) at photon energies from 4.6 GeV to 5.7 GeV and at angles from zero to four degrees. High precision measurements over a range of Z's, photon energies, and angles will ensure a clean separation of the Primakoff production mechanism from competing photoproduction processes. The improved precision is enabled by (1) the use of quasimonochromatic photons from the TJNAF Hall B tagged photon facility and (2), the development of a hybrid π^o detector consisting of a multichannel lead glass detector with a high resolution insertion.

1 Introduction

The two-photon decay mode of the π^o reveals one of the most profound symmetry issues in QCD, namely, the explicit breaking of a classical symmetry by the quantum fluctuations of the quark fields when they couple to a gauge field. This phenomenon, called anomalous breaking, is of a pure quantum mechanical origin. In QCD there are several observable phenomena that originate from such anomalous breakings or anomalies. There is one anomaly connected with the couplings of the quarks to the gluons. This is the so called axial anomaly by which the conservation of the axial U(1) symmetry of the classical Lagrangian of QCD is broken in the limit where two or more quarks are massless, and the divergence of the corresponding axial-vector current becomes proportional to the product $\vec{E}^a \cdot \vec{B}^a$ of the chromoelectric and chromomagnetic fields. The most notorious effect of this anomaly is that there is no SU(3) singlet quasi Goldstone pseudoscalar in the spectrum of mesons. In fact, the lightest such meson is the η' with a large mass of 958 MeV. The origin of this large mass is primarily due to the axial anomaly. The axial anomaly of interest to us involves the coupling to the photons[1][2]. The π^o couples to the isotriplet axial-vector current $\bar{q}\ I_3\ \gamma_\mu\gamma_5\ q$, where $q = (u,\ d)$, and I_3 is the third isospin generator. On the other hand, if we limit ourselves to two quark flavors, the electromagnetic current is given by $\bar{q}\ (1/6 + 1/2I_3)\ \gamma_\mu\ q$. When coupling to the photon, the isosinglet and isotriplet components of the electromagnetic current lead to an anomaly that explicitly breaks the symmetry associated with the axial-vector current $\bar{q}\ I_3\ \gamma_\mu\gamma_5\ q$, and this in turn directly affects the coupling of the π^o to two photons. The decay amplitude is given by:

$$\frac{N_c}{(4\pi F_\pi)^2}\frac{e^2_{\rm em}}{6}\epsilon_{\mu\nu\rho\sigma}k^\mu k'^\nu\epsilon^{*\rho}\epsilon^{*\sigma}, \tag{1}$$

where N_c is the number of colors, k and k' are the photon momenta, and, ϵ and ϵ' are the photon polarizations. As this amplitude depends on the number of colors in QCD, the $\pi^o \to \gamma\gamma$ decay can be used to test that this number is indeed equal to three. The decay rate is then given by:

$$, (\pi^0 \to \gamma\gamma) = \frac{\alpha^2_{\rm em}N_c^2M_\pi^3}{576\pi^3F_\pi^2}, \tag{2}$$

where $F_\pi = 92.42 \pm 0.26$ MeV is the pion decay constant[8].

The result for the decay amplitude given above is exact in the chiral limit, *i.e.*, when the u- and d-quark masses vanish. In this case, the anomaly is saturated by the π^o pole. However, the current-quark masses in the real world are of the order of 5 MeV. There are two sources of corrections due to this explicit breaking of chiral symmetry. The first, and most important, does not change the form of the amplitude given above. It merely replaces the value of F_π in the chiral limit by the measured value determined from π^+ decay[3]. This is a manifestation of the so-called non-renormalization theorem of the anomaly due to Adler and Bardeen. The second is a correction whose origin is in the contributions to the saturation of the anomaly by excited meson poles (π' for instance). These contributions are suppressed with respect to the π^o contribution by a factor of the order of $M_q/M_{\rm meson}$, where $M_q \simeq 5$ MeV is the light quark mass. In Chiral Perturbation Theory such corrections manifest themselves through terms of negative intrinsic parity of order p^6 in the effective Lagrangian.

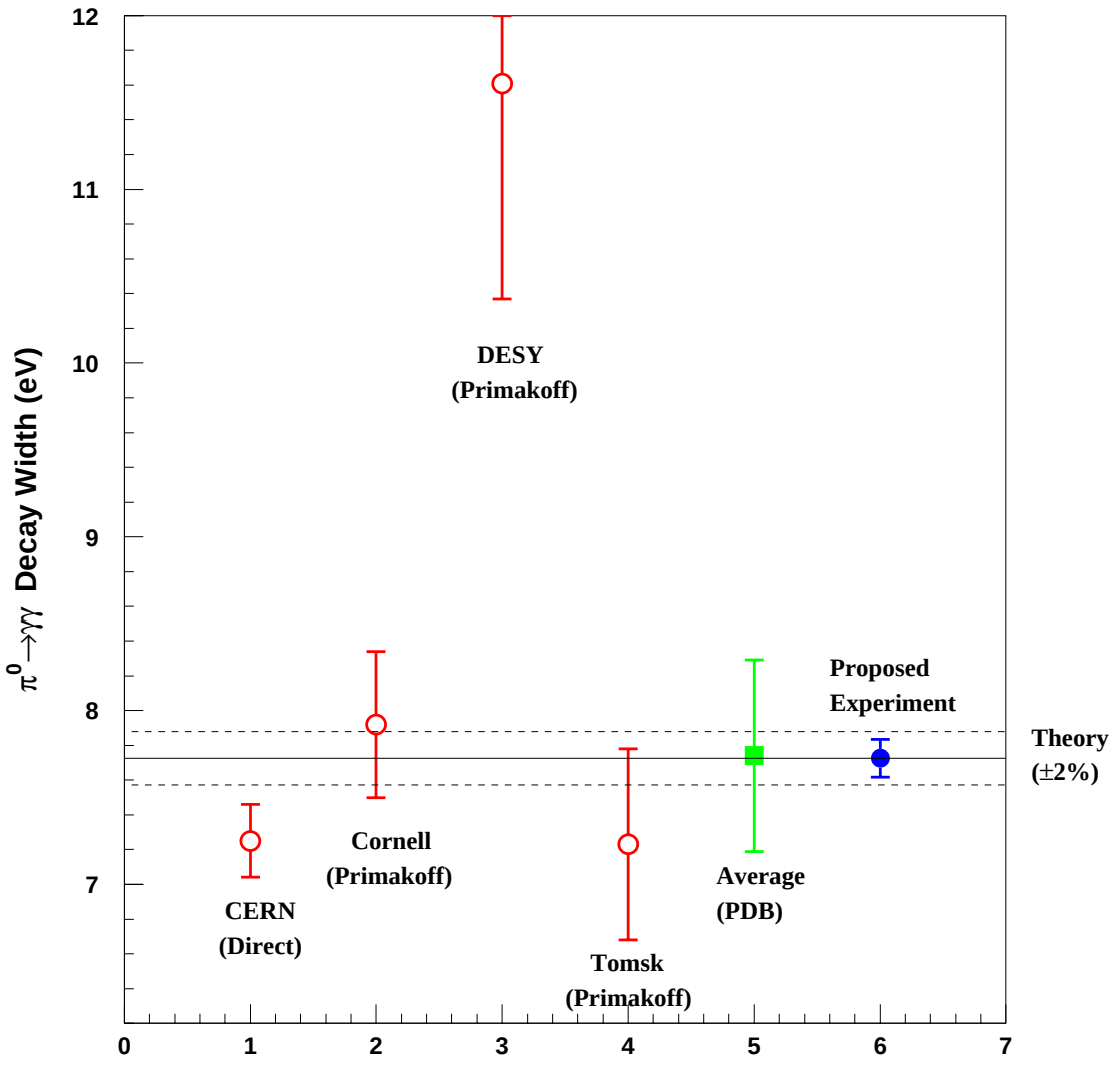

Figure 1: $\pi^o \to \gamma\gamma$ decay width in eV. The horizontal line is the prediction of the chiral anomaly with an estimated 2% error [7]. The experimental results with errors are for : 1) the direct method (CERN) [12] and the Primakoff method: 2) Cornell[15], 3) DESY[16] and 4)Tomsk[17]; 5) Particle Data Book Average [8] based on the experimental points 1), 2), 3) and 4); 6) the expected result for this experiment.

These terms in the Lagrangian have effective coupling constants that cannot be known a priori, and therefore theory cannot predict these corrections. Any observed deviation from the amplitude (1) will probably be due to the p^6 terms mentioned above. The size of such terms have been calculated in extended Nambu-Jona-Lasinio models[6]. The authors find an increase of 0.8% or 1.3% to the π^o decay width in two different versions of these models[6].

In conclusion a measurement of , $(\pi^0 \to \gamma\gamma)$ with an error of $\simeq 1.4\%$, as proposed here, is a fundamental test of the predictions of the chiral anomaly[9, 1, 2]. This is the most accurate prediction in QCD, which depends only on the number of colors. It is arguably the most fundamental experiment that can be performed with few GeV electrons!

2 Previous experiments

The present experimental knowledge of the π^o width is summarized in figure 1[7][8] along with the projected error bar of the proposed experiment. In this figure the predictions of the chiral anomaly (Equation 2)[1, 2, 9], along with the $\simeq 2\%$ theoretical uncertainty due to loop corrections, are presented. Three general experimental techniques have been used to access the neutral pion width: the direct method, $\gamma\gamma$ collisions, and the real Primakoff effect. In addition, a future experiment planned for Hall A of TJNAF [10] will measure the slope of the pion form factor $F_{\gamma\gamma^*\pi^o}(q^2)$ at low q^2 using the small angle scattering capabilities of the Hall A Møller polarimeter.

2.1 The direct method

Direct measurement of the π^o lifetime is made by observation of the decay distance between the production and decay points. This has proven difficult because of the high spatial resolution which is required due to the short lifetime, $\tau \simeq 10^{-16} sec$. In order to be able to discern distinct production and decay points, one must take advantage of relativistic time dilation to get the pion to survive long enough in the laboratory frame. Additionally, good knowledge of the spectrum of the produced pions is necessary in order to extract the lifetime via this method.

The first measurement utilizing such a technique was performed at the CERN PS in 1963 [11]. The precision achieved was 17%. This experiment is not used in the particle data book average. In 1985, an improved version of this technique was employed at the CERN SPS. In this experiment, a 450 GeV/c proton impinged upon two tungsten foils whose separation was variable. The first foil served as the π^o production target and the second foil converted the π^o decay photons to electron-positron pairs. The positrons were subsequently detected. For a small foil separation, some of the π^o's decayed after the second foil, whereas for a large separation, essentially all of the π^o's decayed before the second foil. Thus, by measuring the positron rates for three different foil spacings ranging from 5 to 250μm, the authors were able to determine the lifetime. The dominant systematic errors arise from uncertainties in the π^o spectrum which was not measured but was assumed to be the arithmetic mean of the π^+ and π^- spectra. In addition, corrections had to be made for the Dalitz decay of the π^o's, conversion of the photons in the π^o production target, prompt positron and photon production, and positrons from the decay of η's. A pion lifetime of $\tau_{\pi^o} = (0.897 \pm 0.022 \pm 0.017) \times 10^{-16}$ seconds was obtained[12], corresponding to a width of , $_{\pi^o} = (7.34 \pm 0.18 \pm 0.11)$ eV.

It is interesting to note that this experiment, the most precise of those performed to date, gives a result which is smaller than the chiral anomaly prediction[1, 2, 9]. Also note that the loop corrections tend to increase the predicted width. As such, this experiment provides impetus for a more precise measurement employing a different technique.

2.2 Measurements using $\gamma\gamma$ collisions

The π^o width has been measured using electron-positron collisions at DESY via $e^+e^- \rightarrow e^+e^-\gamma^*\gamma^* \rightarrow e^+e^-\pi^o \rightarrow e^+e^-\gamma\gamma$ [13]. The incident leptons are scattered at very small

angles, and are not detected in the final state. In so doing, they radiate quasireal photons which couple to the π^o which is subsequently identified in an invariant $\gamma\gamma$ mass spectrum. The photons were detected using the Crystal Ball detector which consists of a large array of NaI(Tl) crystals providing 93% solid angle coverage. Contributions to the systematic error included luminosity normalization, detector efficiencies, cosmic ray rejection, and beam-gas collisions. The latter effect arises from the production of π^o's via the interaction of the leptons with residual gas in the beam pipe. The resulting width so obtained was $\Gamma_{\pi^o} = (7.7 \pm 0.5 \pm 0.5)$ eV, very close to the prediction of the anomaly but with a relatively large error (see figure 1).

2.3 Measurements using the Primakoff effect

The Primakoff effect, *i.e.* photopion production from the Coulomb field of a nucleus (see figure 2), has been used in a number of experiments to study the π^o lifetime [14, 15, 16, 17, 18]. The production of π^o's in the Coulomb field of a nucleus by real photons is essentially the inverse decay $\pi^o \to \gamma\gamma$, and the cross section for this process thus provides a measure of the pion lifetime.

Using bremsstrahlung beams of energy 4.4 GeV and 6.6 GeV at Cornell, Browman, *et al.* [15] measured the Primakoff cross sections on several nuclei and obtained a total decay width of $\Gamma_{\pi^o} = (8.02 \pm 0.42)$ eV. As pointed out in [7] and [13] however, the quoted error, which does not have any contribution from uncertainties in the luminosity or detection efficiency (see Table 1 of [15]), may in fact be an underestimate. An analogous measurement of the η width using the Primakoff effect employing a very similar experimental setup and analysis techniques is not in agreement with other experiments.

In view of both the strong theoretical interest in the subject as well as the recent availability of high intensity, high energy tagged photon beams in Hall B of TJNAF, a high precision, state-of-the-art measurement of the π^o lifetime is desirable. In particular, the Hall B tagged photon facility will enable a measurement which will hold two distinct advantages over previous measurements involving bremsstrahlung beams: (1) the quasimonochromatic nature of the tagged beam will enable a clean kinematical separation of the Primakoff mechanism from various background processes, and (2) the tagging technique will enable significantly better control over systematic errors associated with the photon flux normalization.

3 The proposed experiment

We propose to use the quasimonochromatic photons of energy 4.6–5.7 GeV from the Hall B photon tagging facility to measure the absolute cross section of small angle π^o photoproduction from the Coulomb field of complex nuclei. The invariant mass and angle of the pion will be reconstructed by detecting the π^o decay photons from the $\pi^o \to \gamma\gamma$ reaction.

For unpolarized photons, the Primakoff cross section is given by[16]:

$$\frac{d^3\sigma_P}{d\Omega} = \Gamma_{\gamma\gamma} \frac{8\alpha Z^2}{m^3} \frac{\beta^3 E^4}{Q^4} |F_{e.m.}(Q)|^2 \sin^2\theta_\pi \qquad (3)$$

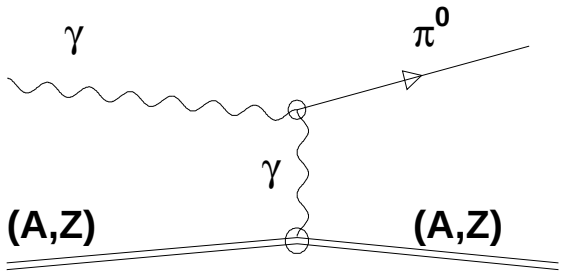

Figure 2: Schematic representation of the Coulomb photoproduction of neutral pions (Primakoff effect).

where , $_{\gamma\gamma}$ is the pion decay width, Z is the atomic number, m, β, θ_π are the mass, velocity and production angle of the pion, E is the energy of incoming photon, Q is the momentum transfer to the nucleus, $F_{e.m.}(Q)$ is the nuclear electromagnetic form factor, corrected for final state interactions of the outgoing pion.

As the Primakoff effect is not the only mechanism for pion photoproduction at high energies, some care must be taken to isolate it from competing processes. In particular, the total cross section is given by:

$$\frac{d^3\sigma}{d\Omega_\pi} = \frac{d\sigma_P}{d\Omega} + \frac{d\sigma_C}{d\Omega} + \frac{d\sigma_I}{d\Omega} + 2 \cdot \sqrt{\frac{d\sigma_P}{d\Omega} \cdot \frac{d\sigma_C}{d\Omega}} cos(\phi_1 + \phi_2) \tag{4}$$

where the Primakoff cross section, $\frac{d\sigma_P}{d\Omega}$, is given by equation (3). The nuclear coherent cross section is given by:

$$\frac{d\sigma_C}{d\Omega} = C \cdot A^2 |F_N(Q)|^2 sin^2\theta_\pi \tag{5}$$

and the incoherent cross section is:

$$\frac{d\sigma_I}{d\Omega} = \xi A(1 - G(Q)) \frac{d\sigma_H}{d\Omega} \tag{6}$$

where A is the nucleon number, $Csin^2\theta_\pi$ is the square of the isospin and spin independent part of the neutral meson photoproduction amplitude on a single nucleon, $|F_N(Q)|$ is the form factor for the nuclear matter distribution in the nucleus, corrected for final state interactions of the outgoing pion, ξ is the absorption factor of the incoherently produced pions, $1-G(Q)$ is a factor which reduces the cross section at small momentum transfer due to the Pauli exclusion principle, and $\frac{d\sigma_H}{d\Omega}$ is the π^o photoproduction cross section on a single nucleon. The relative phase between the Primakoff and nuclear coherent amplitudes without final state interactions is given by ϕ_1 and the phase shift of the outgoing pion due to final state interactions in the final state is given by ϕ_2.

Kinematical considerations enable one to separate Primakoff from other photopion production mechanisms. The Primakoff cross section is zero for pions emitted along the incident

photon direction, has a sharp maximum at an angle $\theta_\pi \sim m_\pi^2/2E_\pi^2$, and falls rapidly to zero at larger angles. It is proportional to Z^2, and its peak value is roughly proportional to E^4. The nuclear coherent cross section for spin zero nuclei is also zero in the forward direction, has a broad maximum outside the angular region of the Primakoff effect, and falls at larger angles as shown in figures 3 and 4, where the amplitudes are normalized to the data of reference [15] and distortion effects are included as discussed in section 8. It is expected to vary little with energy [16]. Measurements of the nuclear effects at larger angles are necessary to determine the unknown parameters in the production mechanism and thus make an empirical determination of the nuclear contribution in the Primakoff peak region. Consequently, this experiment requires a π^o detector with good angular resolution to eliminate nuclear coherent production, and good energy resolution in the decay photon detection will enable an invariant mass cut to suppress multiphoton backgrounds.

We are planning to take extensive data to test the experimental accuracy of the proposed measurements. These are based on the fact that the production of neutral pions by the Primakoff effect is primarily an electromagnetic phenomenon and is therefore accurately calculated. The main features of the Primakoff effect (listed above) will be used to test the accuracy of our data: 1) We will take data with sufficient angular resolution to check the shape of the Primakoff peak after the coherent nuclear and nuclear-Primakoff interference amplitudes, which will be determined empirically by larger angle data, have been subtracted; 2) three spin zero targets (^{12}C,$^{116}\,Sn$,$^{208}\,Pb$) will be used. These have form factors which have been well studied by electron scattering experiments and can be used to test the Z^2 dependence of the cross section ; and 3) the E^4 dependence of the cross section will be measured in the energy range from 4.6 to 5.7 GeV. The study of the Primakoff peak as a function of these three variables should add a great deal of confidence to the measurement and can be used to empirically determine the systematic errors.

4 Experimental setup

The primary experimental equipment required in the proposed experiment includes: (1) the Hall B photon tagger; (2) 5% r.l. solid π^o production targets (^{12}C, ^{116}Sn, and ^{208}Pb); (3) a pair production luminosity monitor located just downstream of the π^o production target; (4) a 1m $\times$ 1m highly segmented lead glass photon detector for π^o decay photons, with a high resolution insertion in the central region near the beam and a plastic scintillator charged particle veto. (See figure 5.)

4.1 The tagged photon system

The primary advantages of the experiment being proposed here over the previous Primakoff experiments [15, 16, 17, 18] arise from the possibility of using the TJNAF Hall B tagging facility to carefully control systematic errors and reduce backgrounds. First, it is clear that the tagging technique will enable a significantly more accurate knowledge of the photon flux. We estimate that it can be controlled to better than 1% by taking the steps discussed below. Second, due to the strong energy dependence of the Primakoff cross section (E^4), it is critical to have good knowledge of the absolute photon beam energy. In the untagged case

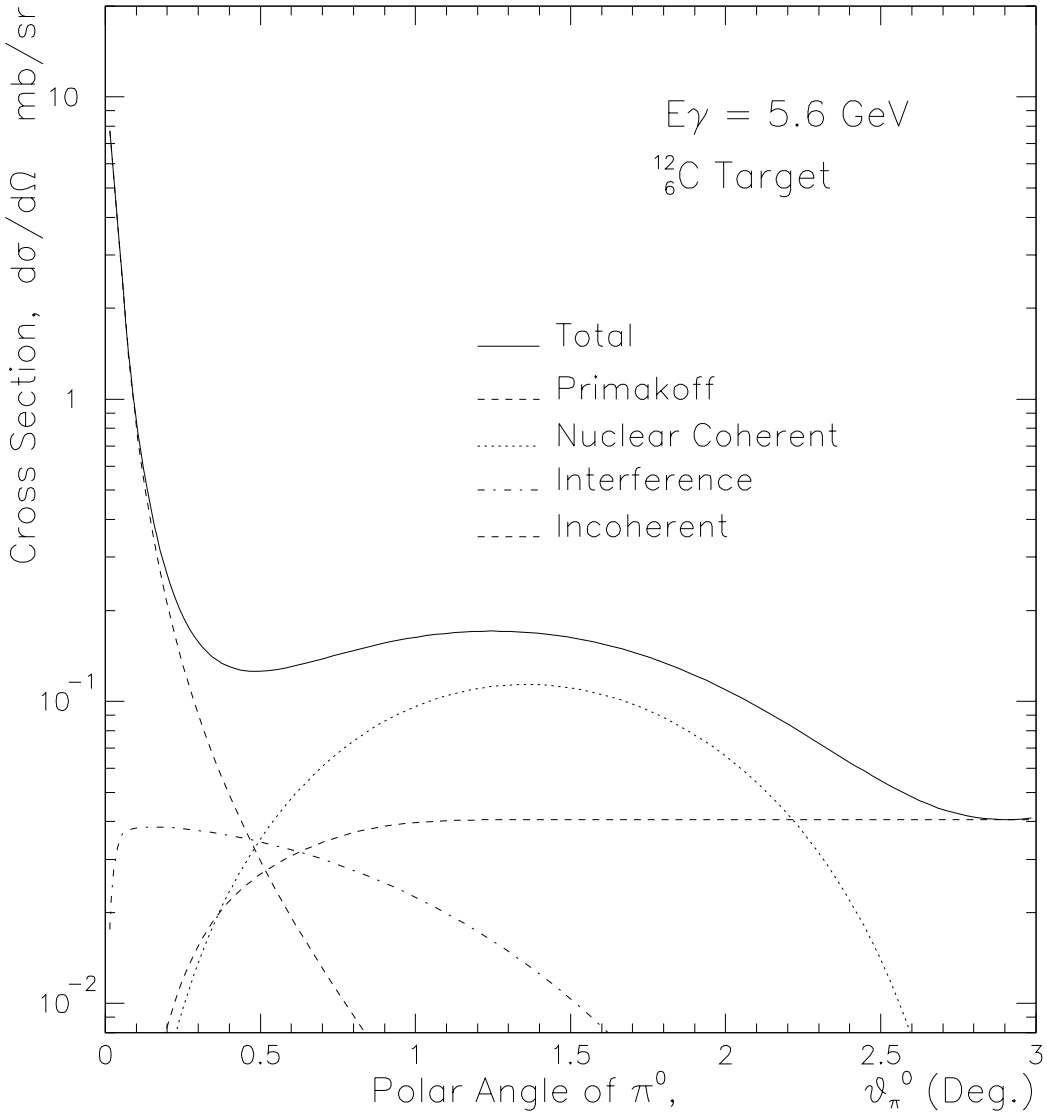

Figure 3: Angular behavior of the electromagnetic and nuclear cross sections for ^{12}C in the 6.0 GeV energy range.

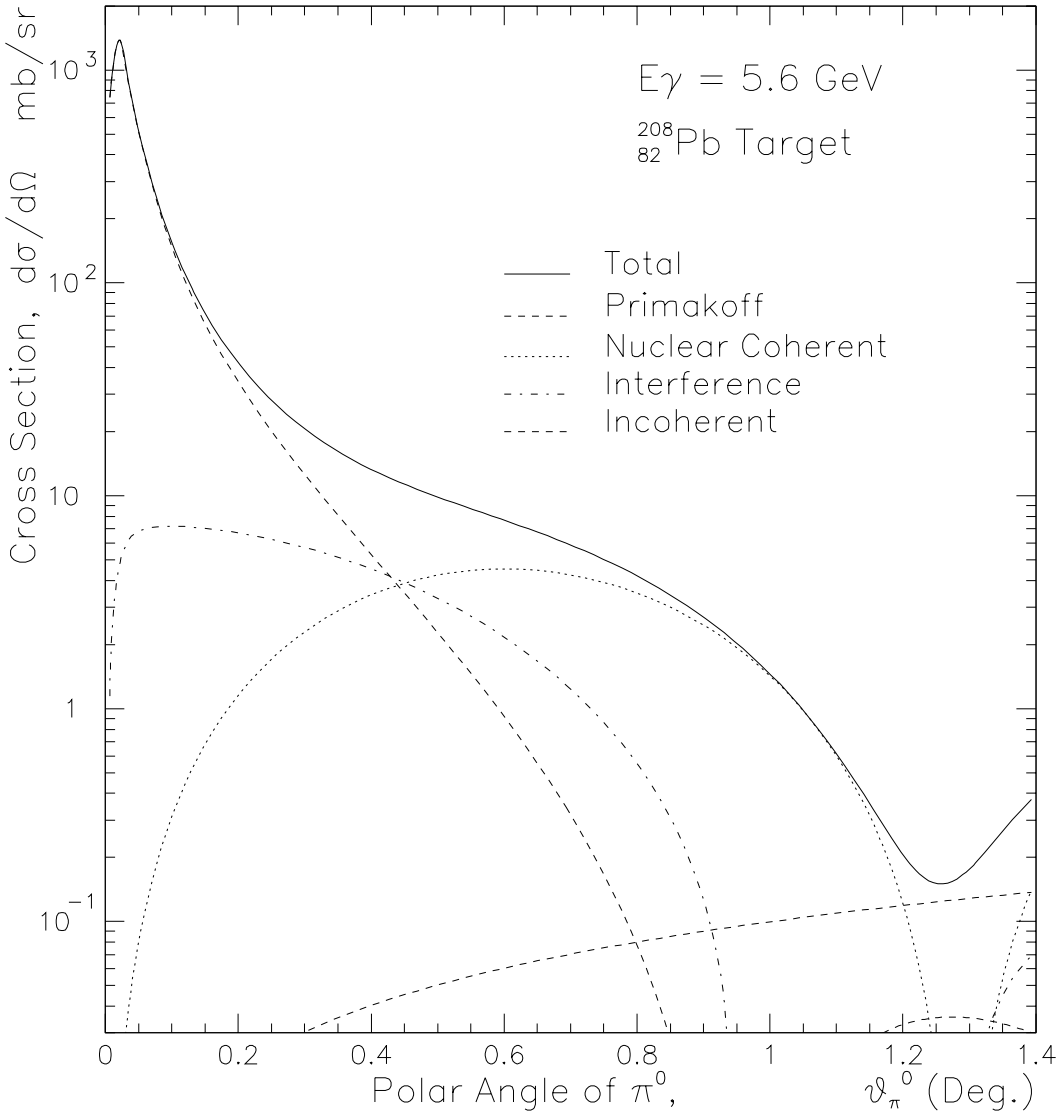

Figure 4: Angular behavior of the electromagnetic and nuclear cross sections for ^{208}Pb in the 6.0 GeV energy range.

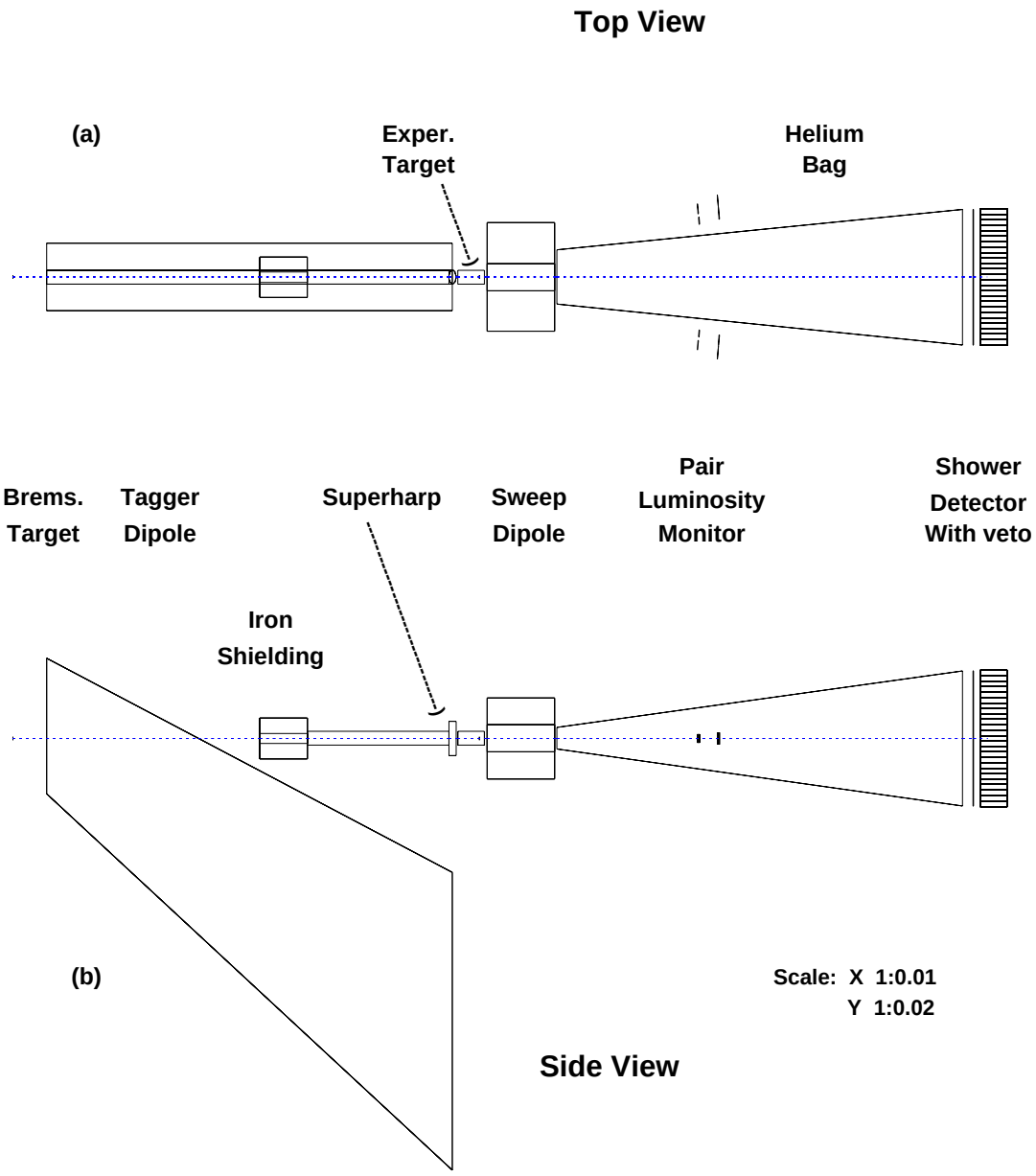

Figure 5: Layout of the experimental setup. (a) Top view. (b) Side view.

of reference [15] it was known to 0.5% and created a 3% uncertainty in the decay width. We anticipate a factor of five improvement in the energy uncertainty at TJNAF.

We propose to use a 6 GeV electron beam incident on a thin (10^{-4} r.l.) bremsstrahlung converter foil. The post-bremsstrahlung electrons will be momentum analyzed in the Hall B photon tagger dipole magnet [19], and photons will be tagged in the energy range 4.6 to 5.7 GeV. (See figure 6). The Hall B bremsstrahlung photon tagging system is equipped with a system of detectors which spans the photon energy range of 20% to 95% of the incident electron energy. The detector system consists of two planes of counters: 384 overlapping scintillators which define 767 fine energy channels of width 0.001 E_e (the "E" counters), and 61 larger scintillators, each read out by two photomultiplier tubes and designed for good time resolution (the "T" counters). The sizes of the T-counters are designed to produce approximately equal counting rates in two groups. When all 61 T-counters are used, the total tagging rate can be as high as 50 MHz for the whole focal plane. Counters T1-T19, which span the photon energy range from 77% to 95% of E_e, are proportionally smaller than the others, and will allow a tagging rate of up to 50 MHz in this region alone. This experiment will use only the "high-rate" counters T1-T19.

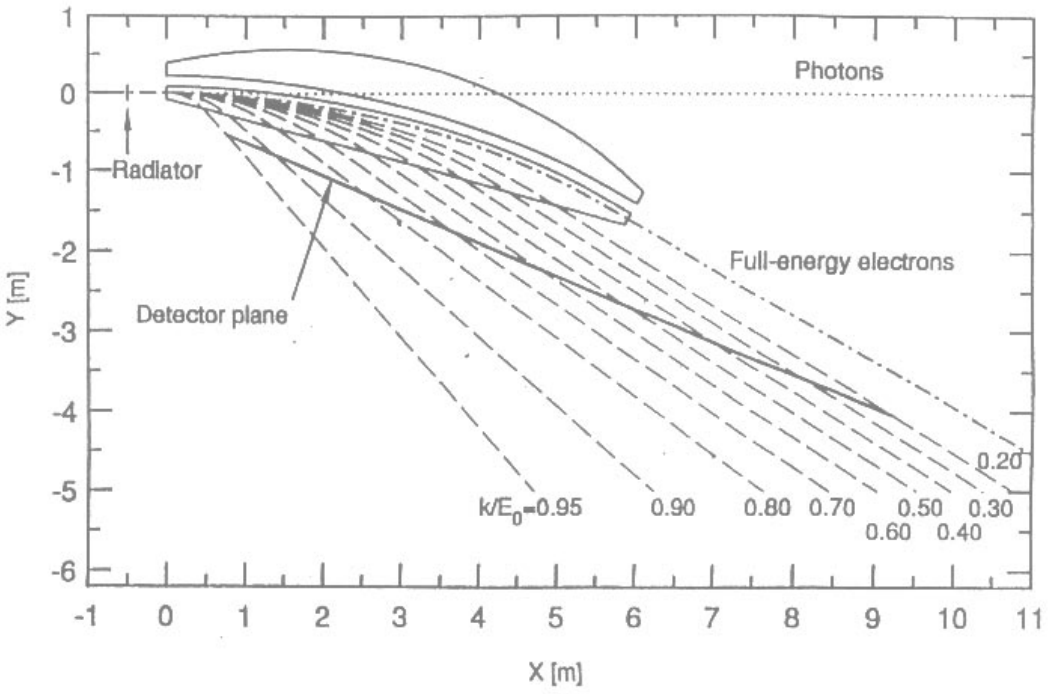

Figure 6: Side view of the Hall B photon tagging system. (Figure is from [19]).

The tagger trigger signal is formed by taking the coincidence of the left and right PMT's of the T-counters. The E-counters will not be included in the coincidence since backgrounds in the tagger are low, and energy information from the E-counters is extracted in off-line

analysis. The tagger Master OR (MOR) is produced by ORing the T-counter coincidence channels.

4.2 The photon beam line

Photons produced in the bremsstrahlung radiator will pass through the 6 cm pole gap of the tagger magnet and then through a 7.5 cm beam pipe. The collimator which is normally used in Hall B experiments will be moved out of position, so that there is no obstruction within 3.75 cm of the beam line until the photon beam hits the Primakoff target approximately 6.5 meters from the radiator. Thus the photon beam is unobstructed out to an angle of about 70 m_e/E_e. Electron beam scans at the position of the radiator are carried out routinely in Hall B experiments, and have shown no measurable halo. For this experiment, we plan to remove the two sweep magnets and the secondary collimator currently on the beam line. We also plan to install a new superharp scanner at the position of the target. A relatively thick wire will be scanned through the photon beam, and secondary particles will be detected downstream using the pair spectrometer system which is described in more detail below. Figure 7 shows a GEANT simulation of the beam profile at the the Primakoff target postion for a 1.5×10^{-3} r.l. gold bremsstrahlung converter. Figure 7(a) shows the beam profile for the full bremsstrahlung beam, and figure 7(b) shows the profile for the high energy component of the beam, $E_\gamma > 5$ GeV, where it can be seen that the expected beam spot is about 1.4 mm. The simulation was checked against the beam profile measured at Bonn[20] using a 1.5×10^{-3} r.l. gold foil and a 1 GeV beam. Excellent agreement was obtained. The photon beam will be steered into Hall B by centering it on a one centimeter scintillator located approximately 50 meters downstream of the radiator in the Hall B alcove. This scintillator should be accurately surveyed and placed on the beamline center.

4.3 Photon flux measurement

Since each π^o decay event is measured in coincidence with a tagged photon signal, the normalization of the cross section to the incident photon flux depends on knowing the number of tagged photons on target in each energy bin during the run. The number of tagged photons on target is not necessarily equal to the number of events recorded by the tagger counters because of two effects: 1) events in which a bremsstrahlung photon is produced but is absorbed before reaching the target, and 2) Møller scattering events in the bremsstrahlung radiator which produce an electron in the tagger counters without an accompanying photon.

Events of the first type will be minimized by allowing the entire bremsstrahlung beam to travel in vacuum without collimation to the target. The second category of events is known to affect the tagging rate at the level of a few percent. The combination of these effects can be measured by removing the Primakoff target and placing a lead glass total absorption counter (TAC) in the photon beam just after the vacuum window downstream of the Primakoff target position, and recording the ratio of Tagger·TAC coincidences to tagger events. Such measurements were made during the photofission experiment performed in Hall B in April 1998. Typically these measurements are made with a 2×10^{-5} r.l. radiator and 0.1 nA beam current. The trigger was the tagger Master OR. Figure 8 shows this tagging

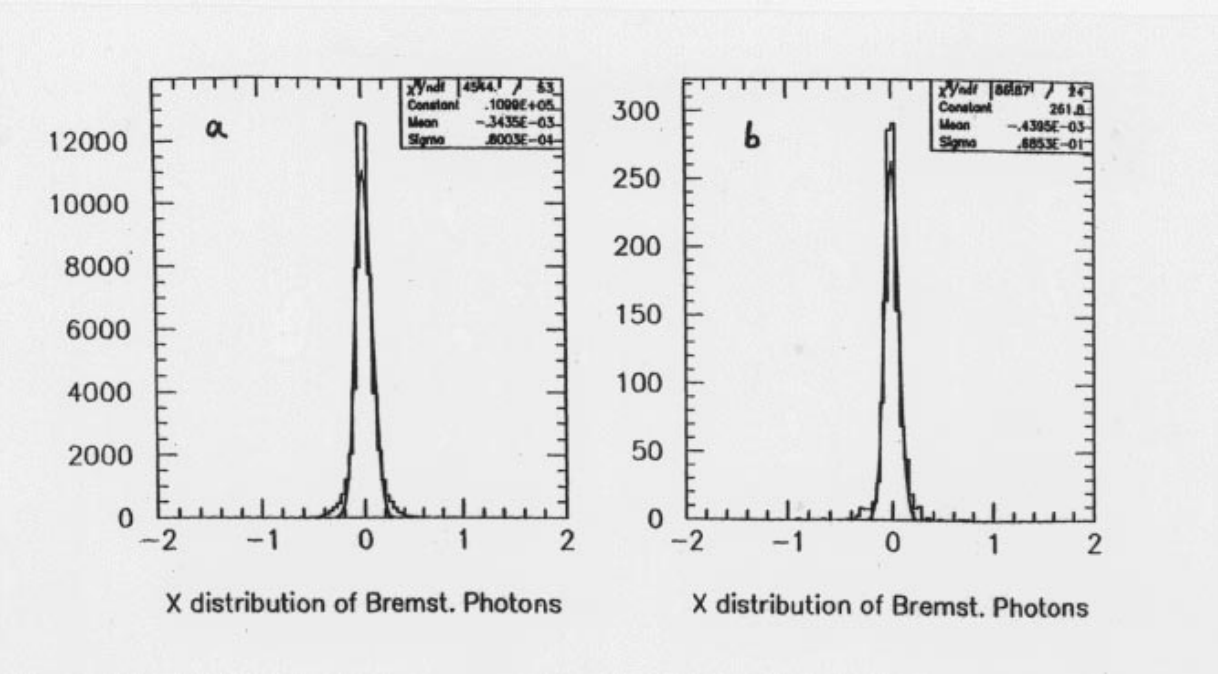

Figure 7: Simulated beam profile at the Primakoff target. (a), Full bremsstrahlung beam. (b), $E_\gamma > 5$ GeV. The x axis is in centimeters.

efficiency ratio at a beam energy of 4.0 GeV. The measured ratio is above 98% except near the endpoint, where the Møller scattering effect is most significant.

Since the TAC can be placed in the beam only at low beam rates and only when the experiment is not taking data, it is necessary to monitor the tagging efficiency by making a relative measurement concurrent with the experiment. This will be done by using the post-target sweeping magnet as part of a pair spectrometer luminosity monitor. The Primakoff target will convert about four percent of the photons into electron-positron pairs which must be deflected enough to miss the π^o detector. Scintillator hodoscopes on both sides of the beam will detect coincidences between electron-positron pairs produced by photons over the full tagged photon energy range of the experiment. These pair spectrometer events will be used in two ways: (1) Hardware coincidences will be made between the pair spectrometer and each of the 19 T-counters of the tagging system, and these coincidences will be counted continuously by scalers. Three sets of scalers will be used: T-counters alone, T-counter-pair spectrometer coincidences, and T-counter-pair-spectrometer delayed coincidences for accidentals subtraction. 2) Each pair spectrometer hodoscope channel will be sent to a TDC, and a secondary trigger will be set up to measure tagger-pair spectrometer coincidences in software. This will allow detailed correlation between the pair spectrometer and the T- and E-counters of the tagging system, so that the flux in each fine energy channel can be monitored continuously. The secondary trigger will be formed by prescaling the left-right pair spectrometer coincidence level down to an acceptable level, approximately 1:1024.

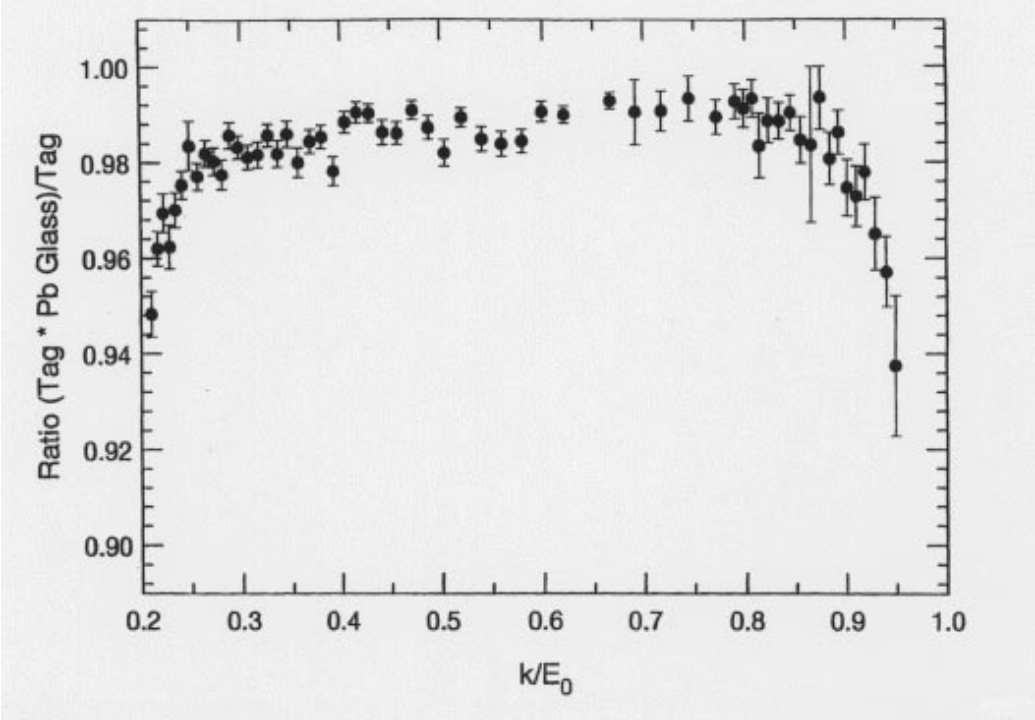

Figure 8: Tagging efficiency across the focal plane of the Hall B tagger as measured in April 1998. The beam energy is 4.0 GeV.

A layout of the proposed pair spectrometer is shown in figure 5. The energy acceptance of the pair production luminosity monitor is shown in figure 9. Figure 9(a) shows the energy distribution of positrons detected in two nonoverlapping plastic scintillator telescopes when an $e^+ - e^-$ coincidence is imposed. Figure 9(b) shows the energy distribution of the corresponding tagged photons. In the simulation, two pairs of telescopes are placed symmetrically on each side of the beam. The larger central peak in (b) arises from the fact that two combinations of left-right coincidences (left inner-right outer or left outer-right inner detectors) feed this peak. The detectors are 3.5 meters downstream of the Primakoff target and consist of 5 mm thick plastic scintillator. The solid angle defining scintillator is 7 cm $\times$ 6 cm. Expected rates are 220 kHz in singles and 36 kHz in coincidence. With this geometry, the $e^+ - e^-$ detection efficiency is quite insensitive to the beam position. A 5 mm shift in the beam corresponds to a 0.3% change in the efficiency. In addition, we plan to control the magnetic field in the dipole sweeping magnet at the 10^{-3} level.

4.4 The π^o detectors

We propose to use a segmented array of lead glass Cherenkov detectors (see figure 9), a 27$\times$27 matrix 1m $\times$ 1m in size, situated 7.5 meters downstream of the π^o production target to detect the π^o decay photons. Each lead glass module will be 4cm $\times$ 4cm $\times$ 40cm, with a total of 608 channels[25]. In addition, we propose to build an array of 2cm $\times$ 2cm $\times$ 15cm $PbWO_4$ crystal detectors[21] in the central region of the array covering 44cm $\times$ 44cm for enhanced coordinate and energy resolution in the region near the beam where photons from

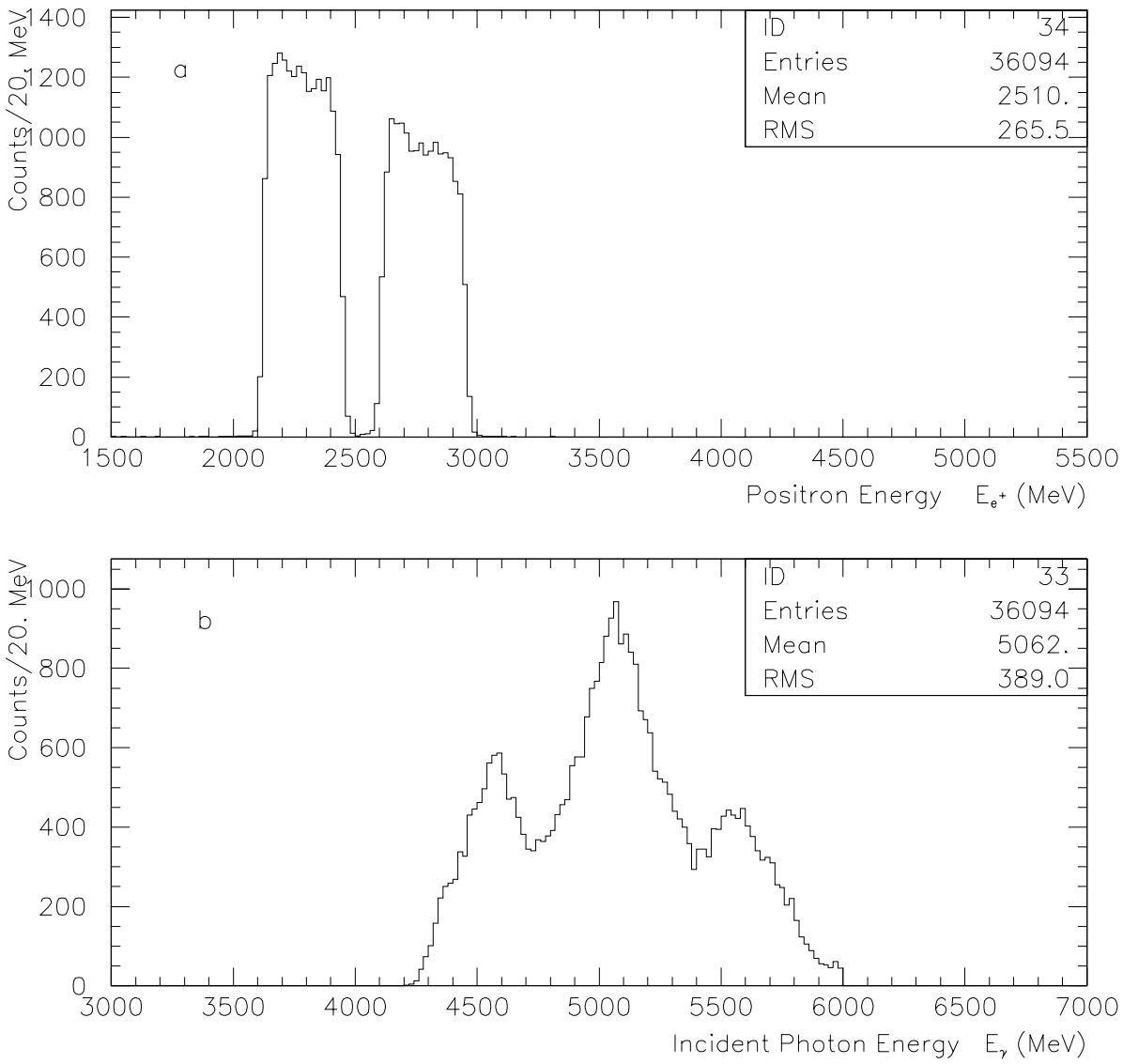

Figure 9: Energy acceptance of the proposed pair production luminosity monitor. (a) Energy distribution of positrons detected in two nonoverlapping plastic scintillator telescopes when an $e^+ - e^-$ coincidence is imposed. (b), Energy distribution of the corresponding tagged photons.

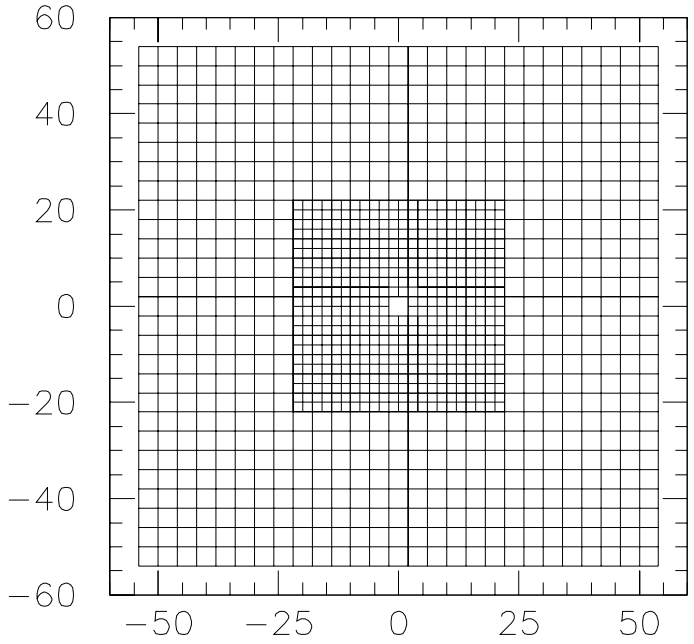

Figure 10: Schematic representation of the proposed hybrid photon calorimeter. The central blocks will be 2 cm × 2 cm $PbWO_4$ crystals and the outer blocks are 4 cm × 4 cm lead glass blocks.

the $\pi^o \to \gamma\gamma$ decay are of higher energy. The addition of the high resolution insertion will significantly improve the invariant mass and angle reconstruction of the pions. In order to control the coordinate and energy resolutions, a multichannel light monitoring system will also be employed.

The central 4cm × 4cm area will be left open to enable the photon beam to pass through. The modules contiguous with this region on the beam axis as well as the two outermost layers of modules in the lead glass wall will be excluded from the fiducial volume of the detector to control coordinate resolution and detection efficiency near the boundaries of the detector. Figure 11(a) shows the distribution of photons under the condition that both of the π^o decay photons hit the physical size of the detector. This corresponds to a geometrical acceptance of 82%. Figure 11(b) indicates the distribution when both photons hit the face of the detector when the central region and the adjacent central blocks are excluded. This cuts the geometrical π^o acceptance to 74%. Figure 11(c) is the hit pattern for the case when each of the photon pair hits the fiducial volume of the detector (*i.e.* with the central blocks and all of the blocks on the two outermost layers excluded). The additional exclusion of the outermost blocks has little effect on the acceptance, as it is reduced to only 73%. Figure 11(d) corresponds to the hit pattern on the entire fiducial volume (as in Figure 11(c)), with the added constraint that the sum of the energy deposition of the two photons exceeds 4 GeV and any given photon deposits at least 0.2 GeV. The additional energy cut has little effect on the geometrical acceptance as it remains at 73%. In order to increase count rates, and to minimize systematic errors associated with correcting for finite acceptance effects, it is

clearly desirable to have a large π^o acceptance. As figure 11 indicates, the main limitation on the acceptance arises from the exclusion of the central modules. Simulations show that excluding an additional ring of blocks (16 in number) around the central region gives an additional factor of about two reduction in acceptance. This places a limitation on how far downstream the detector may be placed from the bremsstrahlung converter. It should be noted in this regard, however, that the smaller Molière radius of the $PbWO_4$ crystals in the central region enables one to extend the fiducial volume of the detector closer to the beamline, thereby increasing the area of coverage in the important central region of the detector.

Figure 12 illustrates the optimum separation between the π^o production target and the lead glass detector. For small separations, approximately 5 meters or less, the π^o detection efficiency falls as a significant number of photons cross the plane of the detector at distances too close to the central axis, and thus do not intersect the fiducial volume. At large separations of the production target and photon detector, the geometrical acceptance falls as photons intersect the plane of the detector outside its outer boundary.

As indicated in figures 3 and 4, one would like to have a large, flat acceptance in θ_π out to at least two degrees to verify that the effect of the coherent nuclear photoproduction amplitude is taken into account adequately. Figure 13 shows the π^o geometrical acceptance as a function of θ_π where this is seen to be the case.

The dipole magnet of the proposed pair production luminosity monitor ($\int B \cdot dl \sim 15$ kilogauss m) will be positioned just downstream of the target and will sweep charged particles away from the π^o detector. In addition, we plan to install a helium bag between the target and the detector to minimize backgrounds. Figure 14 shows the expected power incident on the detector modules which lie in the dispersive (*i.e.* horizontal) plane of the sweeping magnet at the beam height.

Good knowledge of the π^o detector position is essential for obtaining accurate θ_{π^o} reconstruction. We plan to position the π^o detector to an accuracy of 0.75 mm. Overall offsets can be determined by measuring the distribution across the detector of high energy photon singles coming from the Primakoff target. Figure 15 shows the distribution of photons across a horizontal slice of the detector, intersecting the central region through which the photon beam passes. Any offset in the detector with respect to the photon beam will produce a position asymmetry in this distribution of photon singles.

5 Resolutions

Particle identification of the pions will be accomplished by calculating the invariant mass of coincident photon pairs from the experimentally measured quantities E_{γ_1}, E_{γ_2}, and $\psi_{\gamma_1\gamma_2}$, the opening angle between the two photons. The square of the invariant mass is given by:

$$m^2_{\pi^o} = 2E_{\gamma_1}E_{\gamma_2}(1 - cos\psi_{\gamma_1\gamma_2}). \tag{7}$$

Good invariant mass resolution is needed to minimize uncertainties associated with background subtractions. Figure 16 shows the expected invariant mass resolution of our setup for coherent pion production on lead for $E_\gamma = 5.7$ GeV$\pm$0.3% and $\theta_{\pi^o} = 0.1^\circ$, where it can be seen that we expect an experimental resolution of about 3.5 MeV. A number of techniques

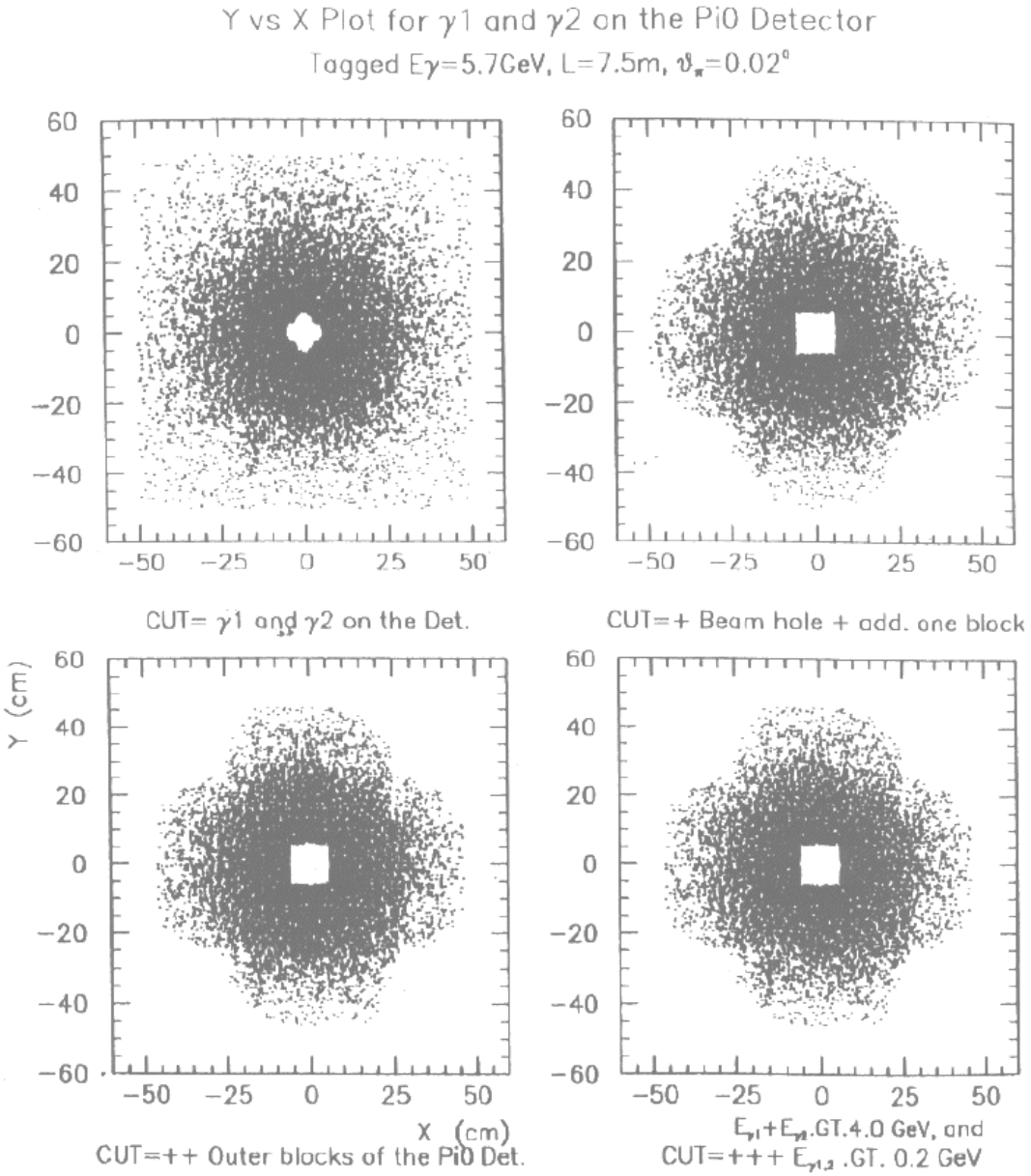

Figure 11: Monte Carlo distribution of two gamma events from π^o decay on the detector for different cut parameters (see text for details).

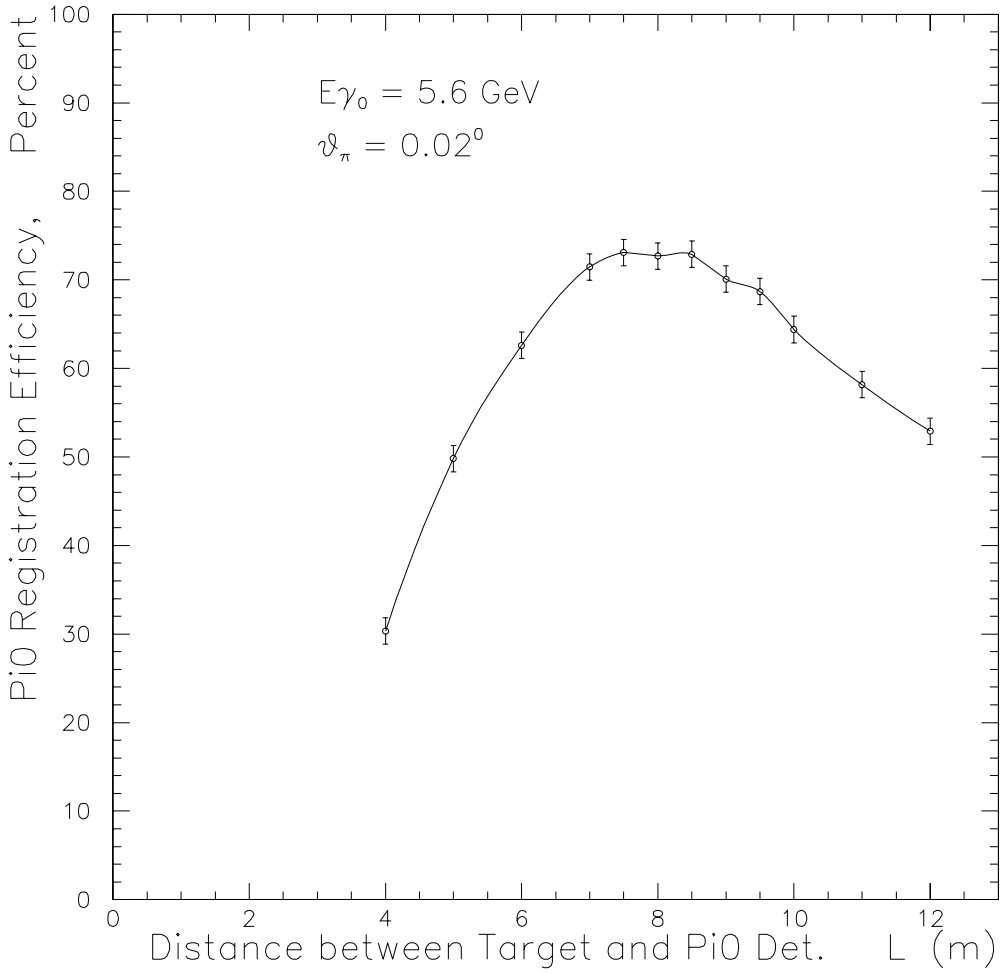

Figure 12: π^o detection efficiency *vs.* distance between the target and photon

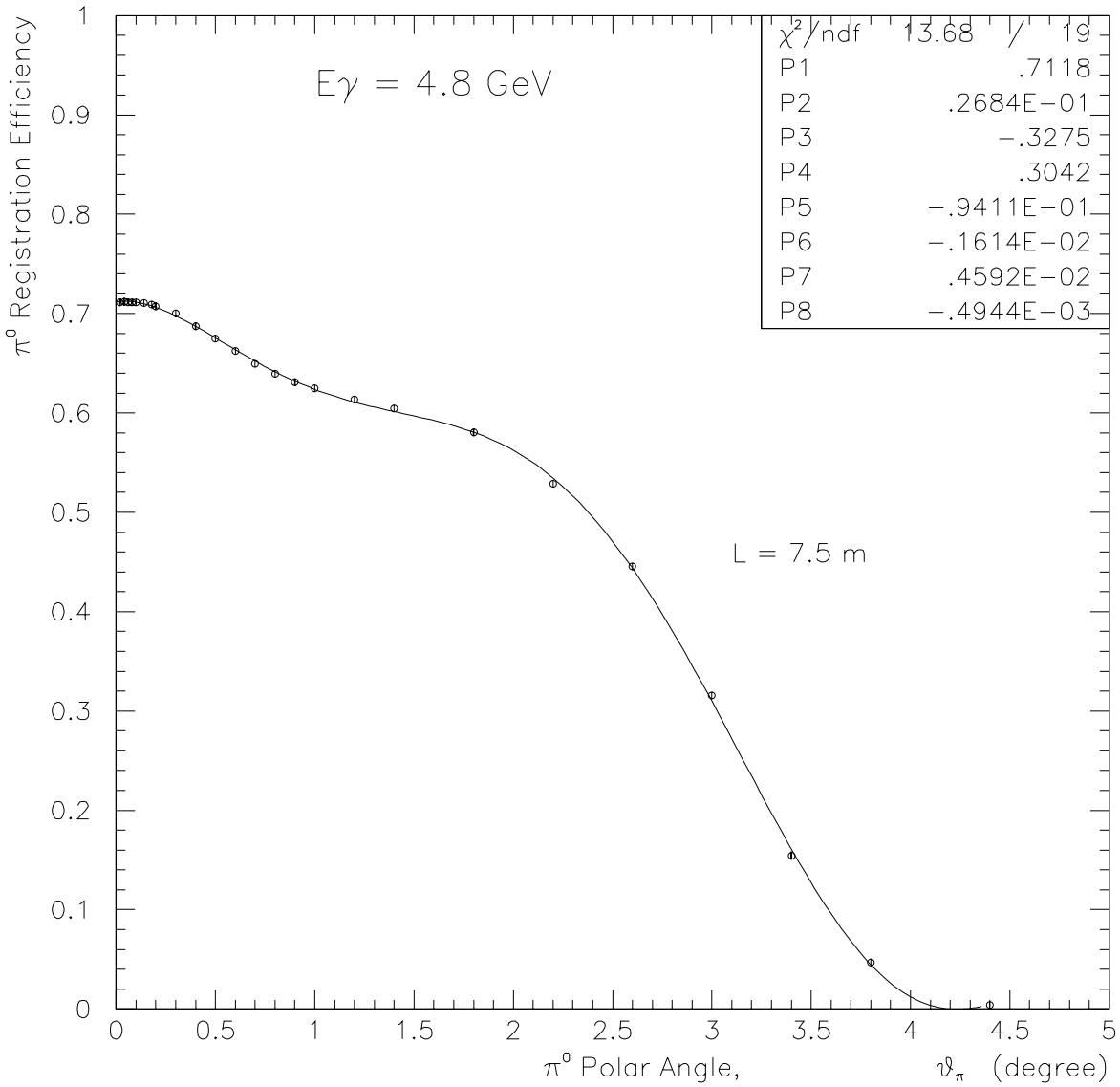

Figure 13: π^o detection efficiency *vs.* production angle. The distance between target and detector is 7.5 m.

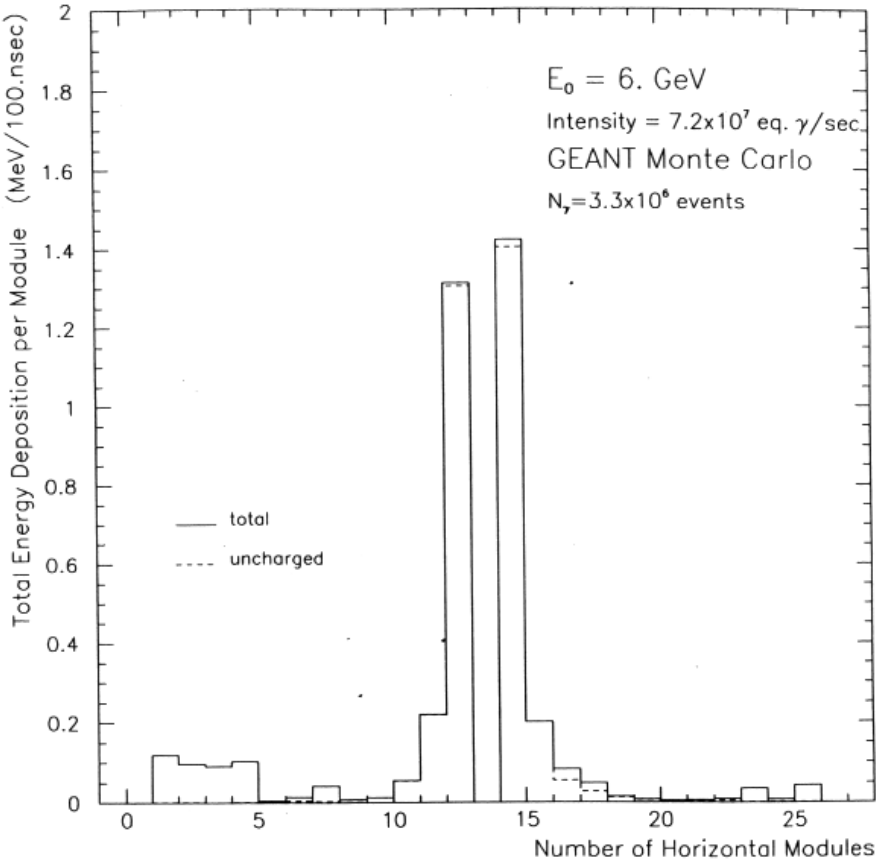

Figure 14: Energy deposition along the horizontal row of detector modules at the beam height. Dashed line is uncharged particles; solid line is charged + uncharged.

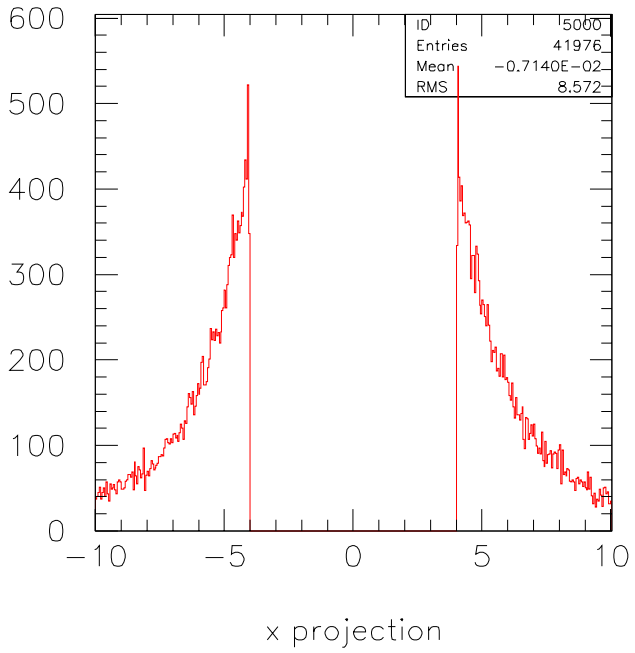

Figure 15: The distribution of photons across a horizontal slice of the central region of the detector.

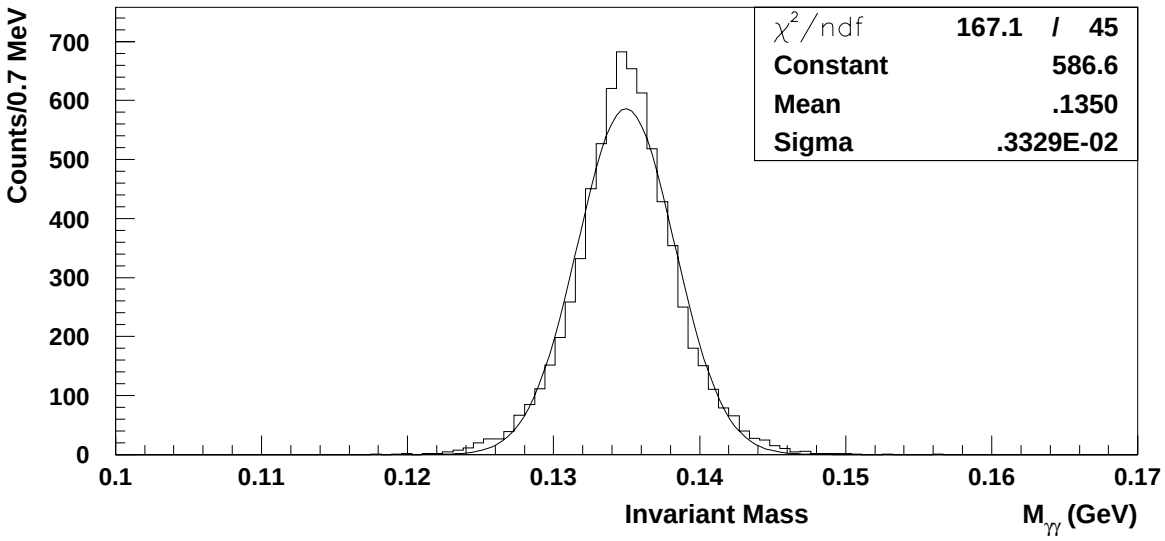

Figure 16: The $M_{\gamma\gamma}$ invariant mass distribution.

for determining the pion energy with the proposed hybrid detector have been examined[22]. The first and crudest method involves simply summing the experimentally measured energies of the two photons. The results of this method are shown in figure 17(a). For the online data analysis, this method will be implemented in the first energy cut on the raw data.

A second method involves the use of the energy sharing between the two photons and the opening angle provided by the experimentally measured coordinate information:

$$E_{\pi^o} = \sqrt{\frac{2m^2_{\pi^o}}{(1-X^2)(1-cos\psi_{\gamma_1\gamma_2})}}, \tag{8}$$

where

$$X = (E_{\gamma 1} - E_{\gamma 2})/(E_{\gamma 1} + E_{\gamma 2}). \tag{9}$$

The results of this method for our detector with the high resolution insertion are shown in figure 17(b), where it can be seen that only marginal improvement is obtained. In general, this method is best suited for photon detectors of poor energy resolution and good angular resolution.

The energy can also be reconstructed using the measured energy of one of the photons and the opening angle:

$$E_{\pi^o} = E_{\gamma i} + \frac{m^2_{\pi^o}}{2E_{\gamma i}(1-cos\phi_{\gamma_1\gamma_2})}. \tag{10}$$

The results of this third method are shown in figure 17(c). As is seen from the figure, the resolution is considerably improved. This is a result of the fact that in most cases the higher energy photon is registered in the high resolution insertion of the detector where coordinate and energy resolution are each a factor of two better than in lead glass. By comparison, if one were to measure the pion energy by the same method but without the high resolution insertion, one obtains a significantly degraded resolution as evidenced in figure 17(d).

Resolution in θ_{π^o} is of particular importance in the identification of the forward peaked π^o's photoproduced by the Primakoff mechanism ($\theta_{\pi^o} \sim 0.02^\circ$) from pions produced at larger angles via the nuclear field (see figures 3 and 4). The pion angle can be determined from the measured photon energies and angles by:

$$cos\theta_{\pi^o} = \frac{E_{\gamma 1}cos\theta_{\gamma 1} + E_{\gamma 2}cos\theta_{\gamma 2}}{\sqrt{E^2_{\gamma 1} + E^2_{\gamma 2} + 2E_{\gamma 1}E_{\gamma 2}cos\psi_{\gamma 1\gamma 2}}}. \tag{11}$$

Figure 18(a) shows the expected angular resolution for coherently produced pions for $E_\gamma = 5.7 \pm 0.3\%$ and $\theta_{\pi^o} = 0.1^\circ$ for a detector consisting of lead glass blocks only. Figure 18(b) shows the improved resolution by implementing the high resolution detector insertion.

The angular resolution under the Primakoff peak can be further improved by means of a kinematical fit, the results of which are shown in figure 18(c). If the incident photon energy is known, and the residual nucleus is left in its ground state as is the case with coherently photoproduced pions, a correlation between the opening angle and the two photon energies results. This correlation is shown in figure 19(a), and the projection onto the $\psi_{\gamma\gamma}$ axis, figure 19(b), gives the opening angle distribution. This additional kinematical constraint results in the improved angular resolution in figure 18(c).

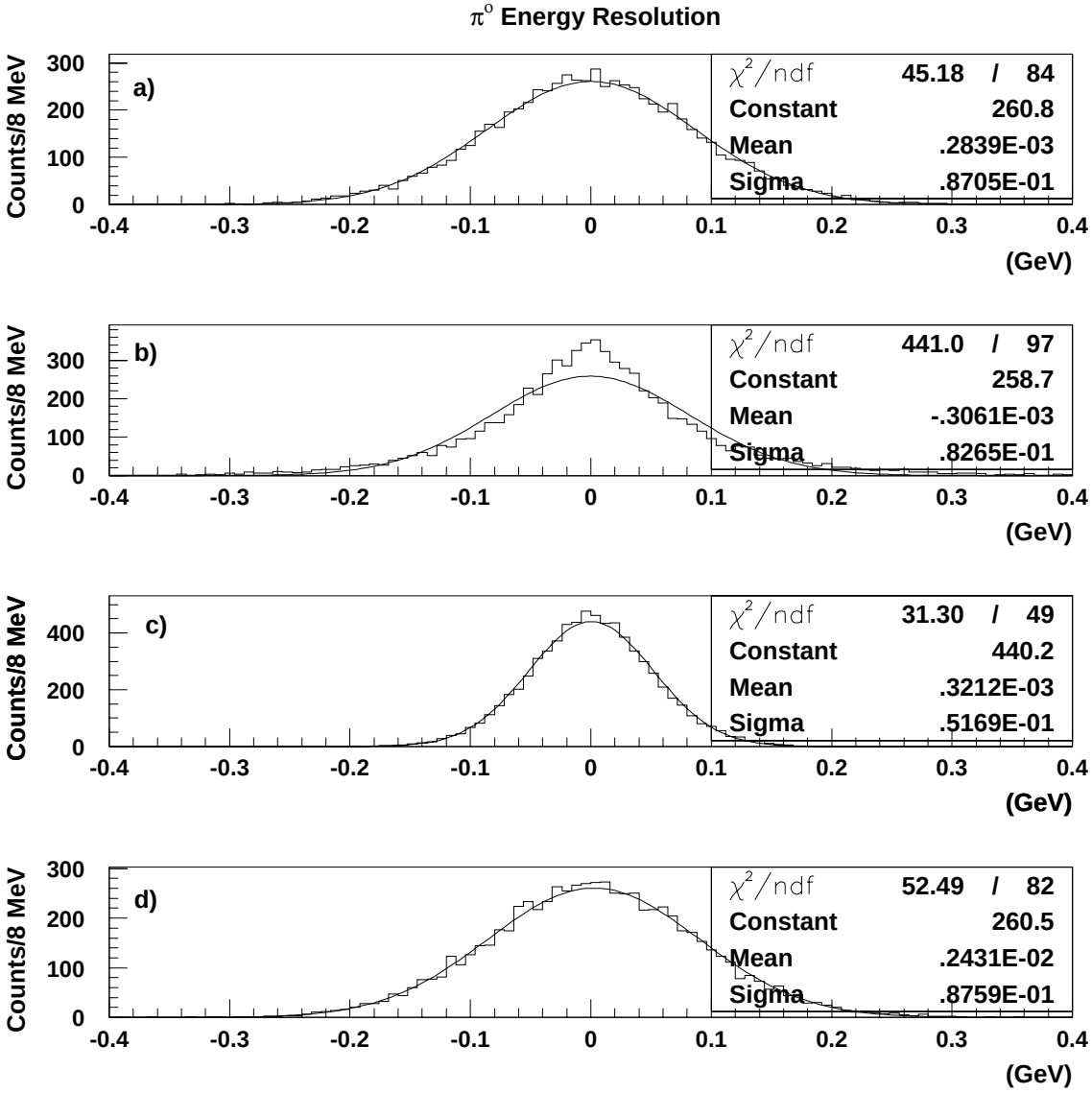

Figure 17: π^o energy resolution for different methods of determining the pion energy. Distribution of events *vs.* $(E_{\pi^o}^{sampled} - E_{\pi^o}^{reconstructed})$ for a) sum of energies; b)energy sharing technique; c)using energy and opening angle; d) same as method (c), but without the high resolution detector insertion.

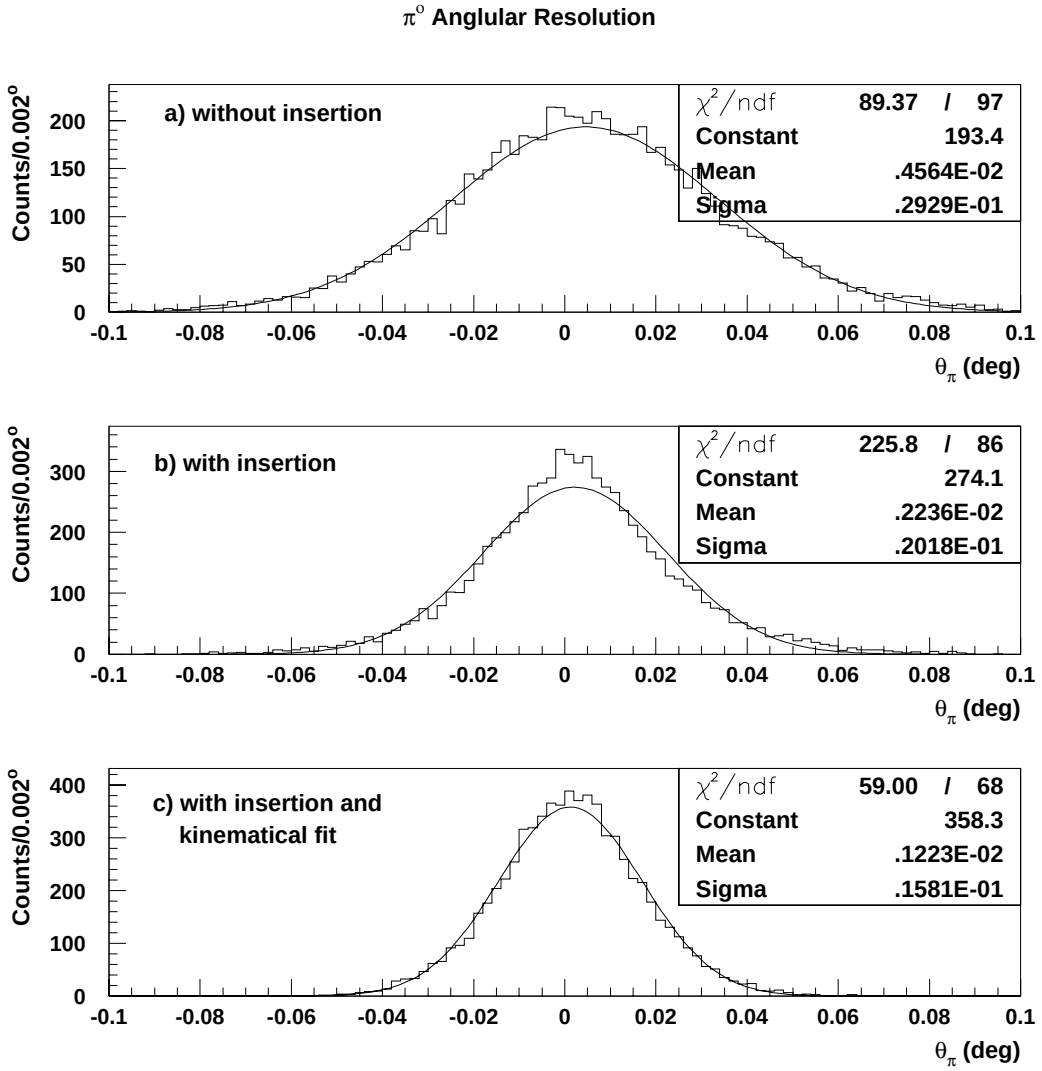

Figure 18: π^o angular resolution. Distribution of events *vs.* $(\theta_{\pi^o}^{sampled} - \theta_{\pi^o}^{reconstructed})$ a) without high resolution insertion; b) with high resolution detector insertion; c) with high resolution detector insertion and kinematical fit.

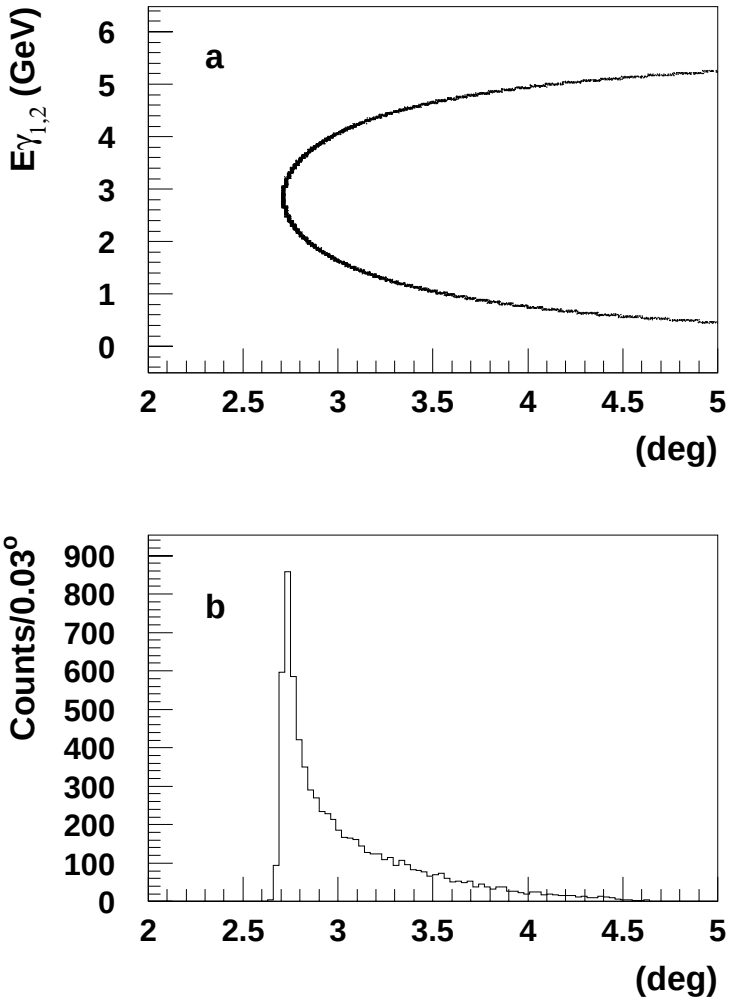

Figure 19: a) Correlation between photon opening angle and two photon energies; b) Opening angle distribution.

The design of the proposed π^o detector has been motivated by the fact that the best angular resolution is obtained with the kinematical fit. This technique requires good knowledge of the high energy photon. We have investigated the angular resolution of alternate detector designs using a calorimeter plus a wire chamber to obtain improved position resolution in conjunction with a preshower counter a few radiation lengths thick to convert the photons[23]. Because of the necessity of the preshower counter, the energy resolution of the photons and the resulting angular resolution of the pions in such a detector is significantly degraded in comparison to the hybrid lead glass/$PbWO_4$ detector. As such, we conclude the that calorimeter alone is preferable. It is worth mentioning, however, that a detector composed entirely of $PbWO_4$ blocks would be the best option yet, though more costly.

A further consideration in θ_{π^o} resolution involves the accuracy of which the interaction vertex is known. Figure 20(a) shows the calculated angular resolution for a pointlike photon beam spot size on the target. Figures 20 (b) and 20(c) show, respectively, the progressive degradation in resolution for four and ten millimeter spot sizes. Such considerations argue for a placement of the target as close to the bremsstrahlung converter as is practical, while still providing space for sweeping magnets. We propose placing the π^o production target 6.5 meters downstream of the converter. In order to get good acceptance for pions, this requires that the π^o detector be placed upstream of the CLAS, 14 meters from the bremsstrahlung converter.

6 Count rate estimates and beamtime

A Monte Carlo generation of the events has been done for several nuclear targets. In these simulations all amplitudes contributing to this process were used normalized to the available experimental data for E_γ=6.6 GeV [15]. The expected experimental yields in six day runs for 5% r.l. ^{12}C and ^{208}Pb targets are shown in figures 21 and 22, respectively. The errors shown are for $\Delta\theta_\pi = 0.005^\circ$ bins and are statistical only. A tagged 8×10^6 γ/sec intensity photon beam was assumed for the accepted energy interval $E_\gamma = (0.85 - 0.95)E_o$.

The expected rate for each channel will be about 1 MHz, which is two times less than the maximum design count rate [26]. The total π^o rate for lead integrated for the $\theta_\pi = 0^\circ - 2^\circ$ angular interval, and for the parameters listed above is expected to be:

$$Rate = N_\gamma \times N_{nuclei} \times \Delta\sigma \times E_{eff} \approx \tag{12}$$

$$\approx 8 \cdot 10^6 \times 9.2 \cdot 10^{20} \times 2.16 \cdot 10^{-2} \cdot 10^{-27} \times 0.7 = 9600 events/day. \tag{13}$$

The generated angular distributions were fitted with the following procedure: for each $\Delta\theta_\pi$ bin the number of expected events $n_i(\theta_\pi)$ was calculated for each component of the cross section by folding in the bremsstrahlung spectrum and the detector angular resolution and acceptance. The solid lines on the figures show the result of the fit with the extracted values for all four free parameters. From these data a 0.9% statistical error for the $\pi^o \to \gamma\gamma$ decay width is achieved. In this energy range the magnitude of the nuclear amplitude is small (≤ 2 %, see figure 3 and 4. To test that it has been properly taken into account, we will extract the Primakoff cross section independently for each of the three targets and check that it is proportional to Z^2.

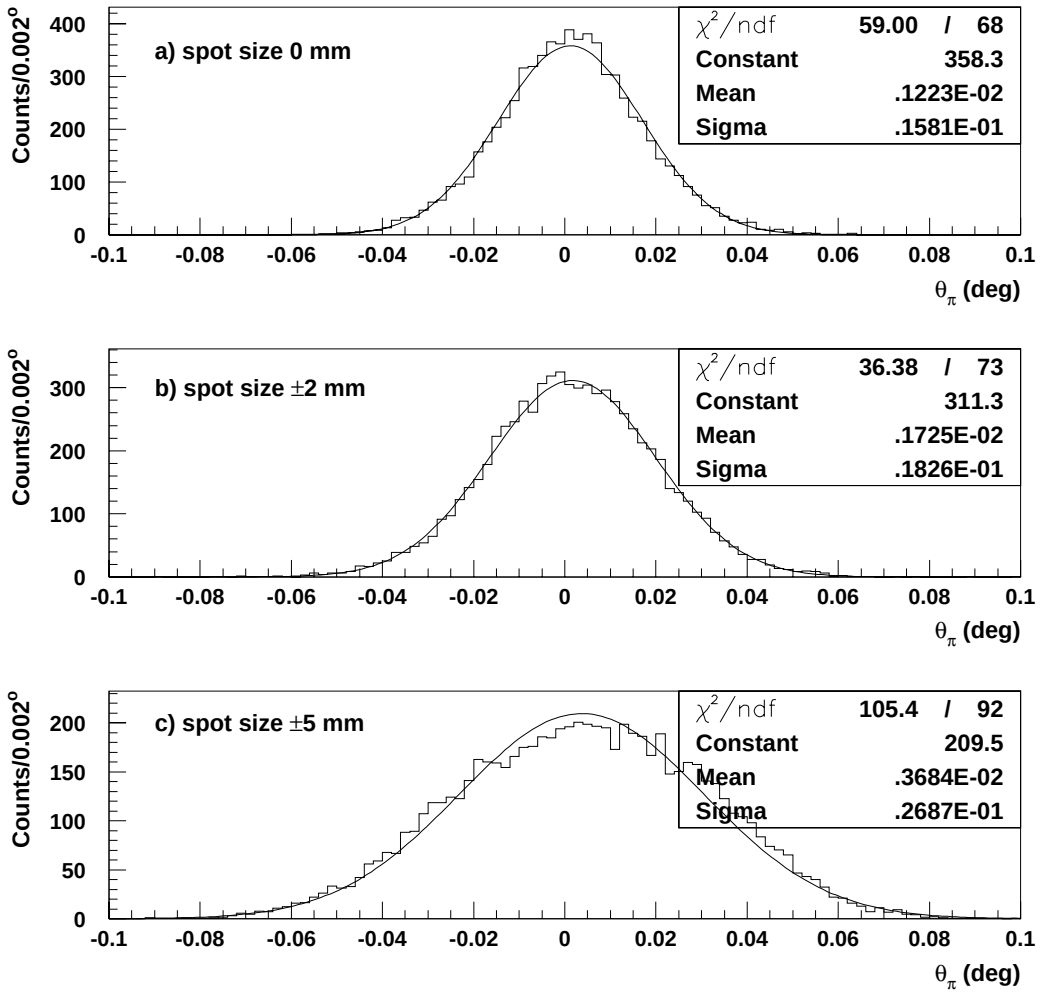

Figure 20: π^o angular resolution for different photon beam spot sizes on the target. Distribution of events *vs.* $(\theta_{\pi^o}^{sampled} - \theta_{\pi^o}^{reconstructed})$ for a) point spot; b) ± 2 mm spot size; c) ± 5 mm spot size.

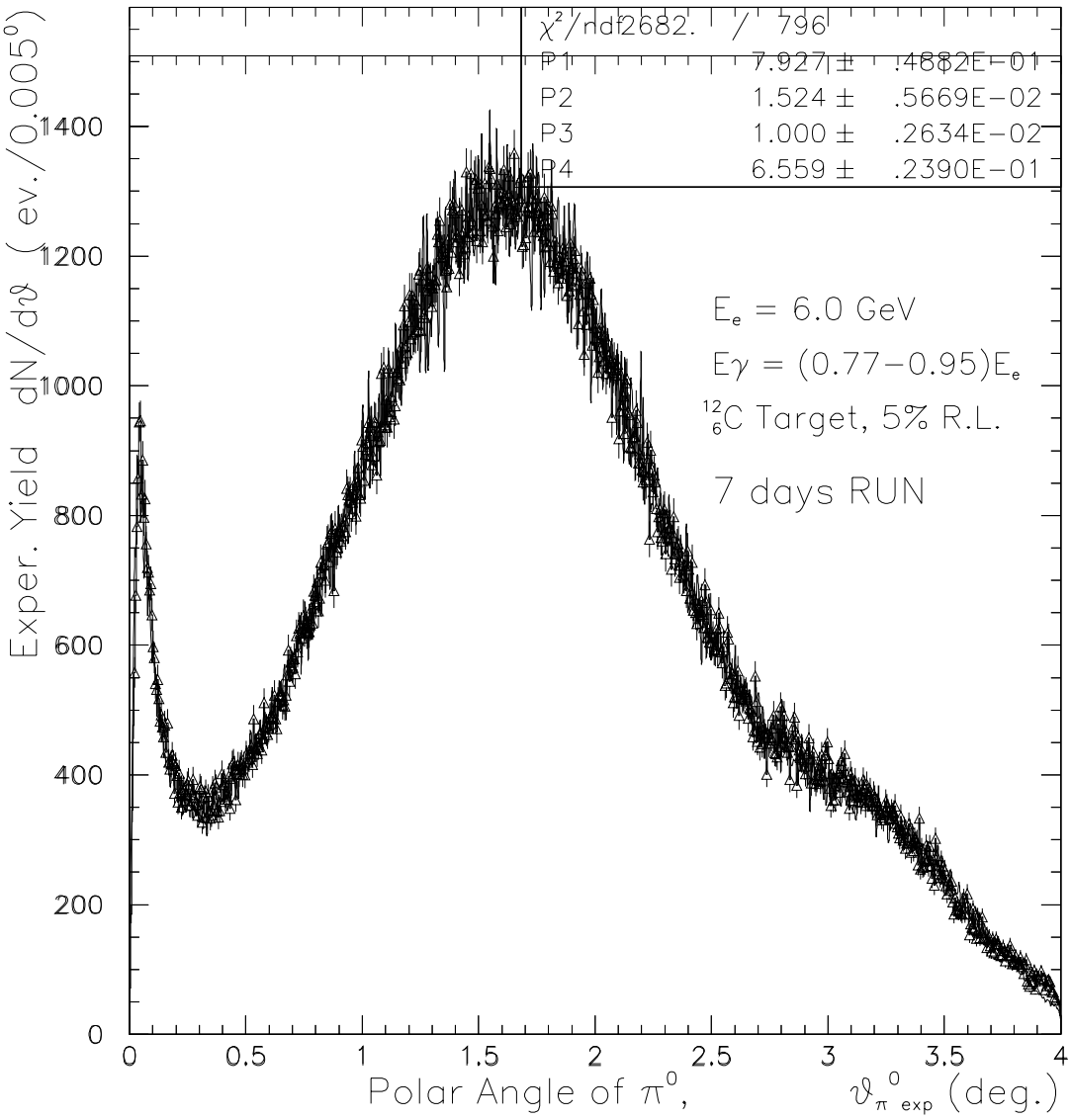

Figure 21: Expected experimental yield *vs.* θ_{π^o} for 6 days of running on carbon.

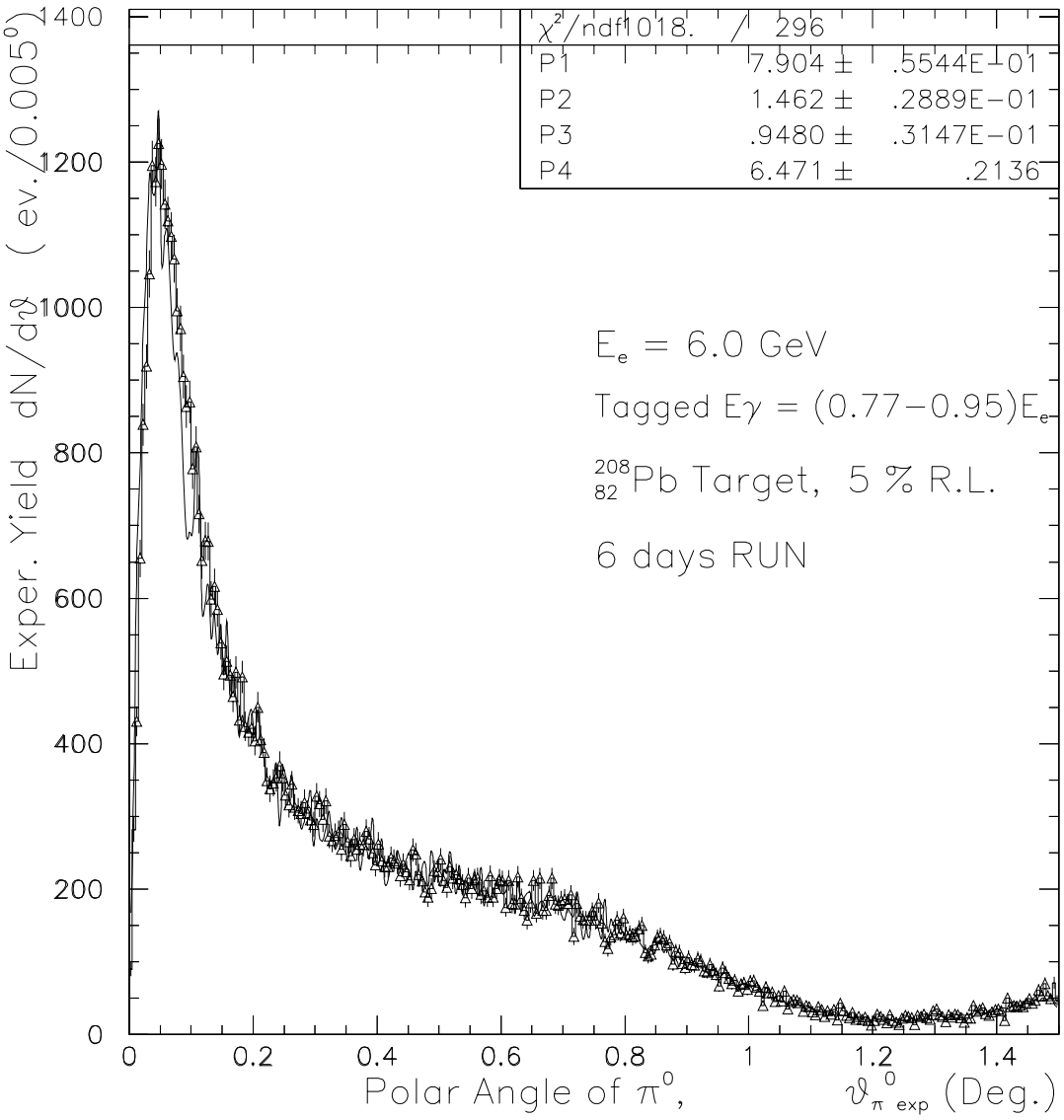

Figure 22: Expected experimental yield *vs.* θ_{π^o} for 6 days of running on lead.

We are requesting a total of 19 days for production data taking – 7 for ^{12}C and 6 each for ^{116}Sn and ^{208}Pb. In addition, we estimate three days of beam time will be necessary for the empty target runs and for the calibration of the multichannel lead glass/$PbWO_4$ detector. Therefore, we estimate a total of 22 days of beam time for the determination of the $\pi^o \to \gamma\gamma$ decay width with a statistical error less than 0.5%.

7 Background rates

For high photon energies, the dominant photoabsorption mechanism involves the production of the vector mesons ρ, ω, and ϕ. In this experiment, only the ρ and ω decays are expected to produce measurable π^o rates on the detector. The proposed experiment will greatly reduce the uncertainty due to contamination of the Primakoff signal from the other channels for two reasons. First, the proposed hybrid π^o detector consisting of a wall of lead glass detectors and a high resolution insertion will significantly increase pion angular and energy resolutions, thereby enabling tighter cuts on the Primakoff events. Second, the tagging technique provides a powerful kinematical constraint which was not present in previous experiments employing bremsstrahlung beams. The production cross sections for the ω and ρ have been calculated, and their subsequent decays via $\omega \to \pi^o\gamma$, $\omega \to \pi^o\pi^-\pi^+$, $\rho \to \pi^o\gamma$, and $\rho \to \pi^+\pi^-\pi^o$ have been simulated in GEANT.

The cross section for ω production on complex nuclei is given by:

$$\frac{d\sigma}{dt} = \frac{d\sigma_{A,coh}}{dt} + \frac{d\sigma_{A,incoh}}{dt} \tag{14}$$

The coherent part is given by[27]:

$$\frac{d\sigma_{A,coh}}{dt} = \frac{d\sigma_{Pom}}{dt}(t=0) \cdot e^{Bt} \cdot |A_{eff}^{coh}|^2 \cdot |F(t)|^2 \tag{15}$$

where t is the Mandelstam variable, $\frac{d\sigma_{Pom}}{dt}(t=0)$ is the Pomeron exchange cross section[28], B is taken to be $7\,GeV^{-2}$[28][29][30], F(t) is the nuclear form factor, and $A_{eff}^{coh} = \sigma_T(\gamma A)/\sigma_T(\gamma N)$ is taken from [31].

The incoherent cross section is given by[27][32]:

$$\frac{d\sigma_{A,incoh}}{dt} = [\frac{d\sigma_{Pom}}{dt} + \frac{d\sigma_{OPE}}{dt}] \cdot A_{eff}^{incoh} \cdot G(t) \tag{16}$$

where A_{eff}^{incoh} is the effective number of nucleons contributing to incoherent vector meson production[31], and G(t) takes into account suppression at small t due to nuclear correlations.

The two body decay $\omega \to \pi^o\gamma$ (B.R. 8.5×10^{-2}) was sampled in GEANT, with an angular distribution proportional to $(1 + cos^2\theta_{c.m.})$ [33]. The three body $\omega \to \pi^o\pi^-\pi^+$ decay (B.R. 8.9×10^{-1}) was sampled according to three body phase space. Figure 23(a) shows the missing energy spectrum ($E_\gamma - E_{\pi_o}$) obtained from the simulation of ω photoproduction and subsequent decay for six days of beam time with a lead target. Since the coherent pion photoproduction will appear as a peak near $E_{miss} = 0$ GeV, figure 23(a) illustrates how knowledge of the incident photon energy provided by the tagging technique enables one to greatly minimize contamination of the π^o spectrum. A further reduction is given by the

stringent cut on θ_{π^o} enabled by the high resolution detector insertion. Figure 23(b) shows the angular distribution of π^o's both with and without the four sigma missing energy cut indicated in figure 23(a). As the experimental θ_{π^o} distribution arising from photoproduction via the Primakoff mechanism will be confined to $\theta_{\pi^o} < 0.2^\circ$, a further substantial reduction in ω background is obtained.

The ρ photoproduction cross section was taken to be ten times the ω cross section[32][34] and the resulting pion detection acceptance from the decays $\rho \to \pi^o\gamma$ (B.R. 7.9×10^{-4}) and $\rho \to \pi^o\pi^+\pi^-$ (B.R. $< 1.2 \times 10^{-4}$) were simulated. Figures 24(a) and 24(b) show the resulting missing energy and θ_{π^o} spectra for six days of running on lead, where in figure 24(b), the rates with and without the four sigma missing energy cut are also indicated.

Figure 25 shows the expected total π^o angular distribution for ρ and ω photoproduction, along with the expected yield from the Primakoff mechanism, where missing energy cuts have been imposed.

7.1 Accidentals

Figure 26(a-c) shows the spectrum of single γ events from (a)$\omega \to \pi^o\gamma$, (b)$\omega \to \pi^o\pi^+\pi^-$, and (c) the total singles rate from the omega. The singles rates for the ρ were calculated to be 1.4% that of the omega. A summary of the expected singles rates is shown below:

$\omega \to \pi^o\gamma$	0.1 Hz
$\omega \to \pi^o\pi^+\pi^-$	0.7 Hz
$\rho \to \pi^o\gamma$	0.01 Hz
total singles (GEANT)	3.3 kHz
total accidental rate (GEANT)	4.0×10^{-2} Hz
π^o signal rate	0.11 Hz
raw trues/accidentals	2.8

The quoted accidental rate represents raw trigger accidental coincidences between the π^o detector and the photon tagger. When invariant mass, missing energy, and opening angle cuts are applied, the accidentals are expected to be negligible. The rates from GEANT are derived from a simulation including the Primakoff target, the pair production luminosity monitor, and the π^o detector. The singles and accidentals rates are shown as a function of single particle threshold in figures 27(a) and 27(b), respectively. These rates include charged particles, as we do not plan to incorporate the charge particle veto which will be in front of the detector into the hardware trigger.

7.2 Correlated $\gamma\gamma$ backgrounds

The decays $\omega \to \pi^o\gamma$ and $\rho \to \pi^o\gamma$ result in three photon states which are correlated in time. Figures 28(a-d) and 29(a-d) show the correlated two photon rates as a function of (a) invariant mass, (b) missing energy, (c) $\psi_{\gamma 1\gamma 2}$, and (d) θ_{π^o}. No cuts are applied in the figures. In figure 28(a), the position and resolution of the π^o invariant mass peak is shown, where the indicated peak height is reduced by a factor of 25 compared to that expected from Primakoff

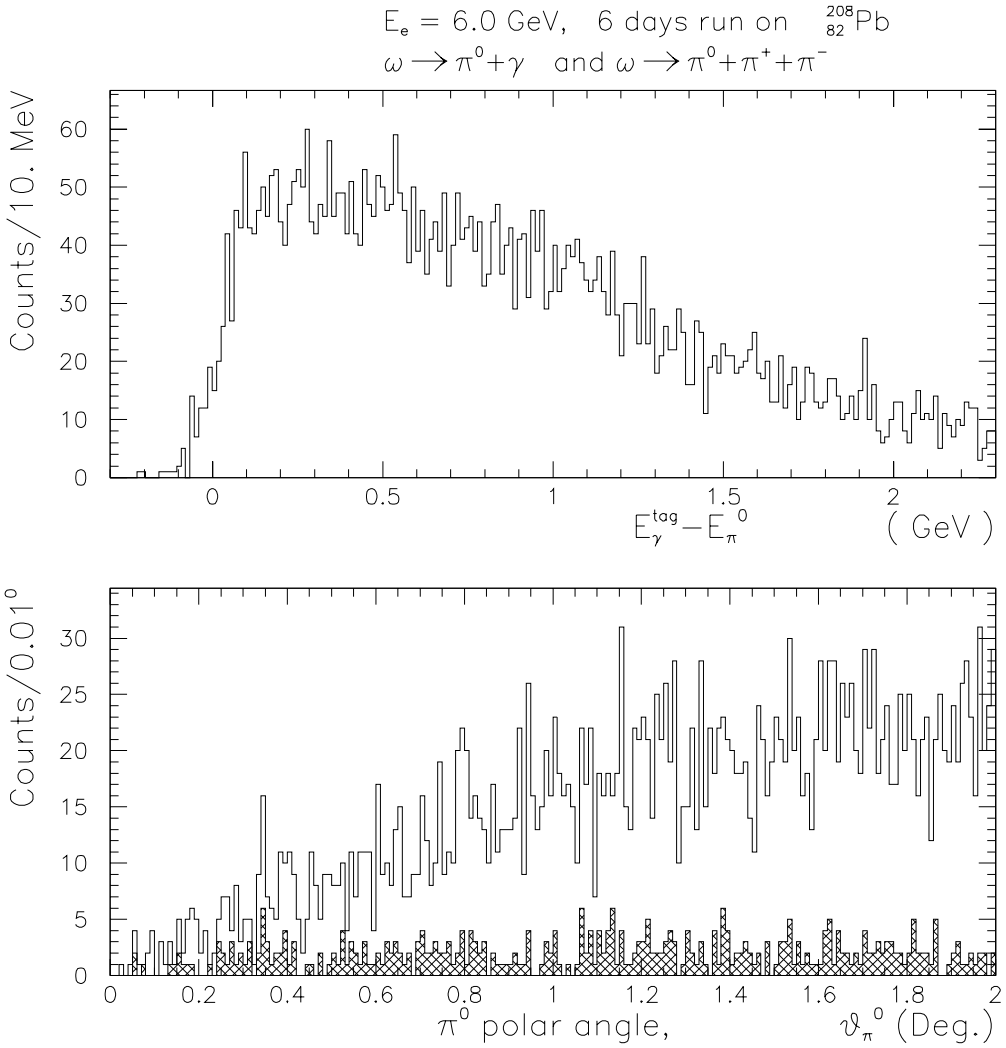

Figure 23: (a) Missing energy spectrum and (b) polar angle spectrum of π^o's from omega decay. Open histograms represent total rates. Cross hatched histogram in (b) represents rates which pass a 4 σ missing energy cut in (a).

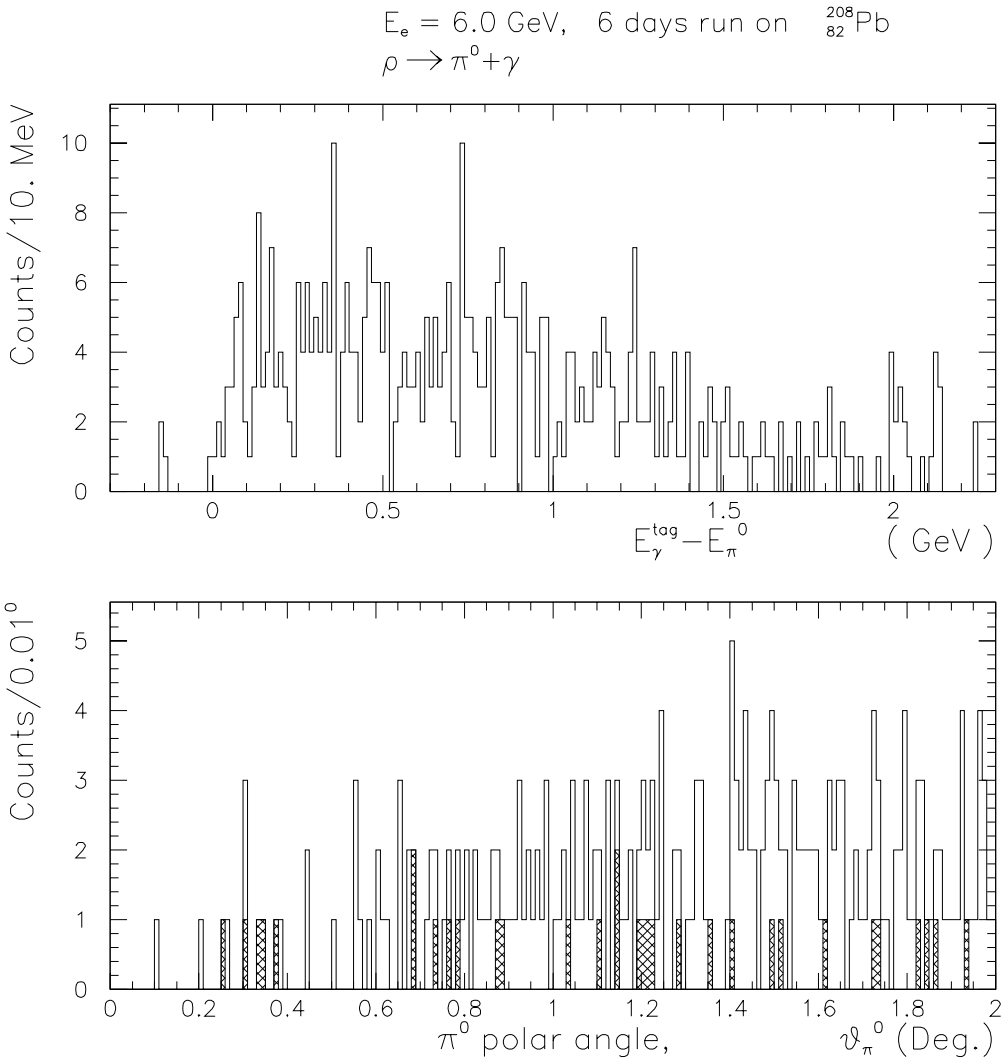

Figure 24: (a) Missing energy spectrum and (b) polar angle spectrum of π^o's from rho decay. Open histograms represent total rates. Cross hatched histogram in (b) represents rates which pass a 4 σ missing energy cut in (a).

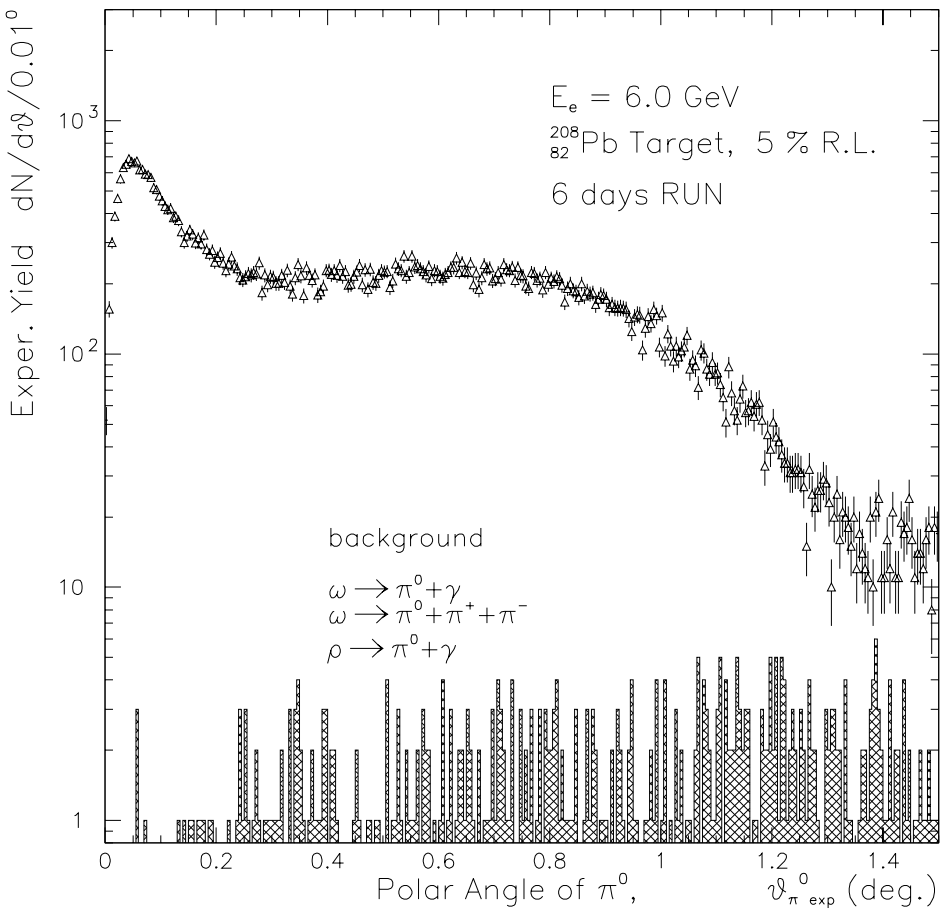

Figure 25: Cross hatched histogram: total π^o background events *vs.* θ_{π^o}. Triangles: Photoproduced π^o's.

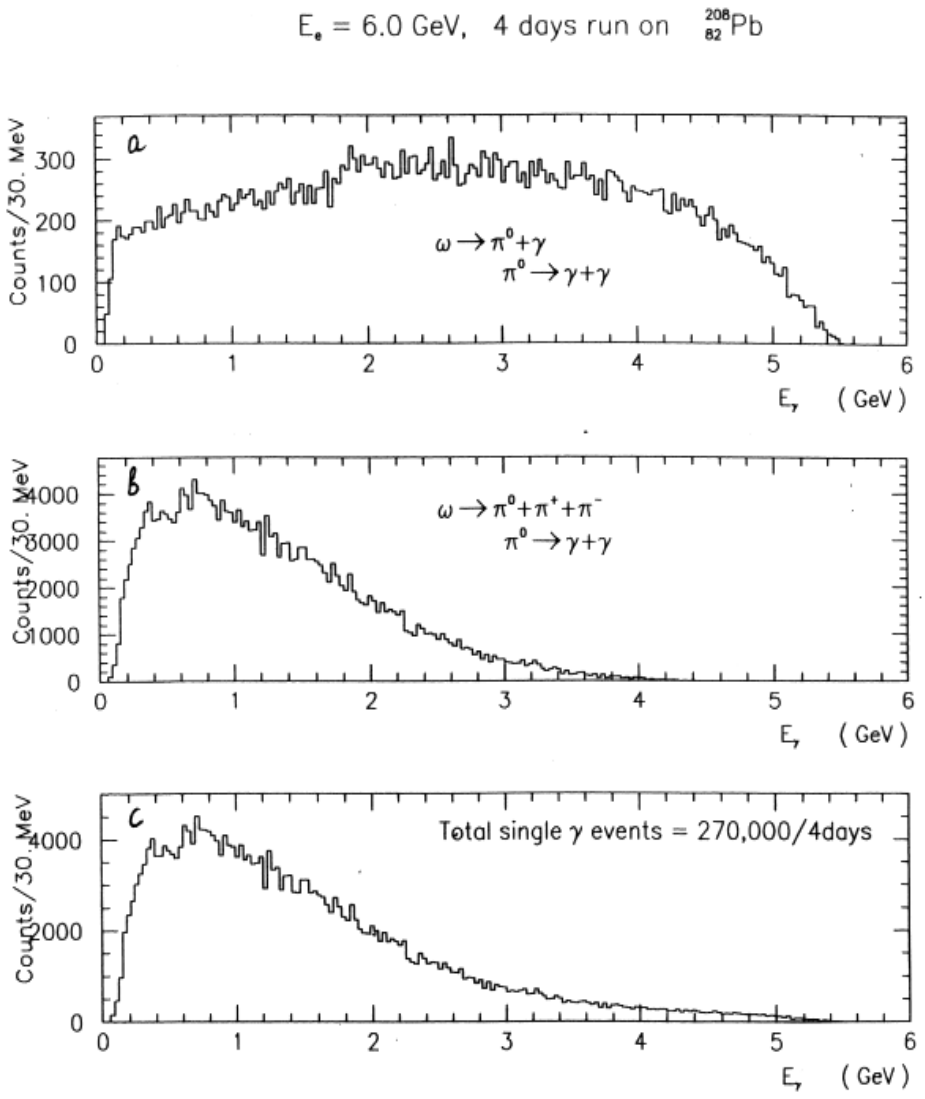

Figure 26: Singles photons expected from four days of running on lead. (a)$\omega \rightarrow \pi^o\gamma$, (b)$\omega \rightarrow \pi^o\pi^+\pi^-$, (c) Total singles from the omega meson.

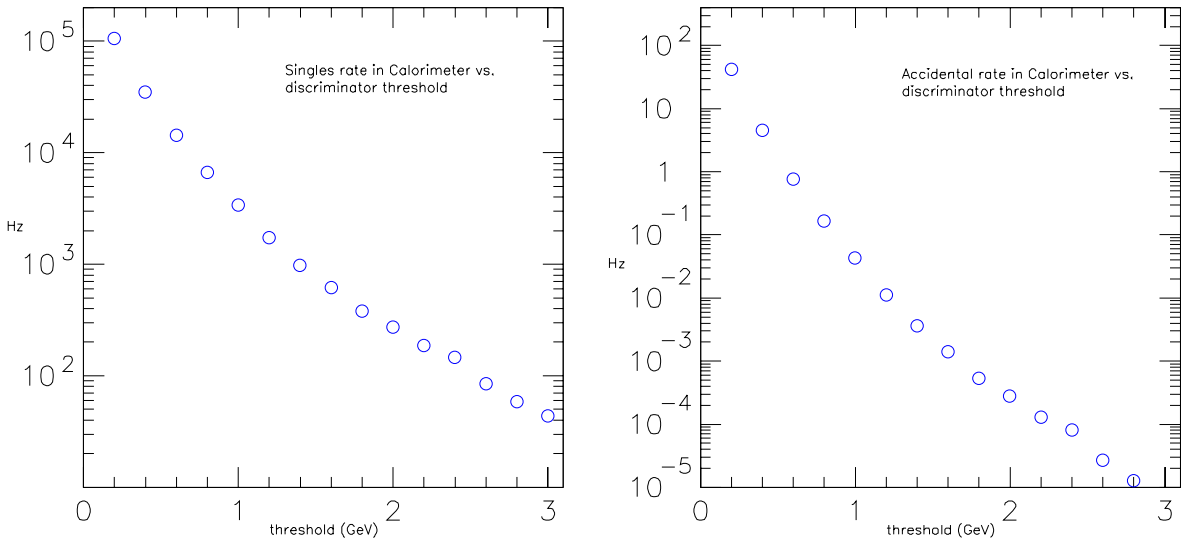

Figure 27: (a)Singles and (b), accidental rates in the π^o detector as a function of single particle threshold.

π^o photoproduction. When π^o invariant mass, missing energy, minimum $\gamma_1\gamma_2$ opening angle, and θ_{π^o} cuts are imposed, these correlated background rates are found to be negligible.

A GEANT simulation which takes into account secondary interactions in the Primakoff target and sweeping magnet indicates correlated two particle rates of around 10 Hz. While these will be present in the raw trigger, the majority of these are due to charged particles which will be vetoed offline.

7.3 π^o backgrounds from the photon beamline

In addition to the Primakoff production target, other sources of π^o's include the bremsstrahlung converter, the pole faces of the tagger magnet (6 cm gap), the 7.5 cm aperture of the iron shielding at the exit of the photon tagger, and the exit window between the pair production luminosity monitor and the π^o detector.

The rate of π^o's produced in the bremsstrahlung converter foil as a function of energy is shown in figure 30. These rates include π^o's produced up to ten degrees due to Primakoff, nuclear coherent, and nuclear incoherent processes. Figure 31 illustrates the acceptance of the π^o detector to these pions under the conservative assumption that all of these pions are emitted at zero degrees. Figure 31(a) shows the sampled spectrum of the pions produced in the bremsstrahlung foil, and figure 31(b) shows the energy distribution of the single photon events which reach the detector. This rate is calculated to be 0.3 Hz. As shown in figure 31(c), the two photon acceptance of pions produced in the converter foil is negligible.

Pions produced in the pole faces and the iron shielding near the exit of the tagger and those produced at the vacuum window between the pair production luminosity monitor and the π^o detector can be distinguished on the basis of their reconstructed invariant mass

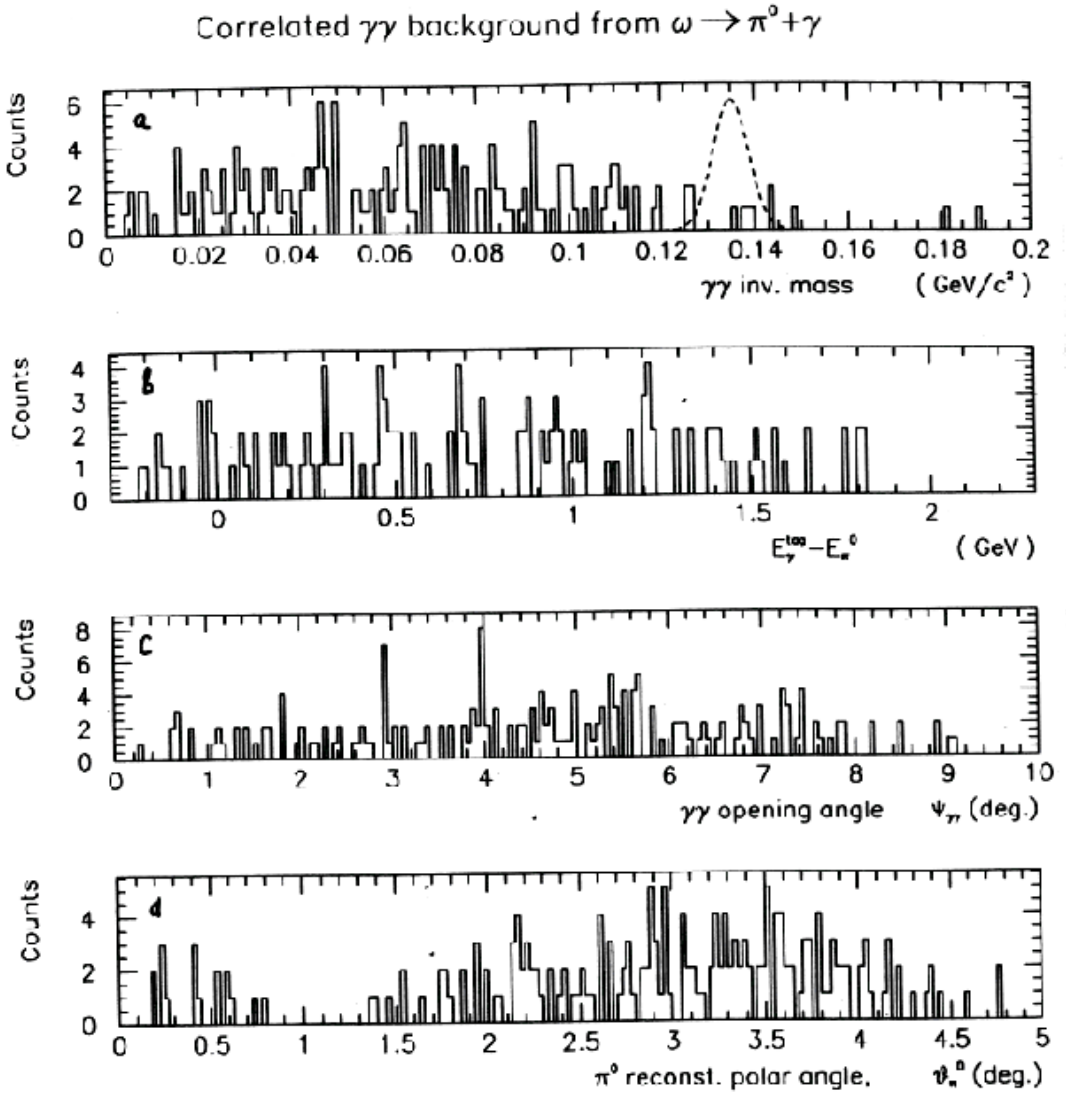

Figure 28: Correlated two photon rates from the omega as a function of (a) invariant mass, (b) missing energy, (c) $\psi_{\gamma 1 \gamma 2}$, and (d) θ_{π^o}. No cuts are applied in the figures. In figure (a), the position and resolution of the π^o invariant mass peak is shown, where the indicated peak height is reduced by a factor of 25 compared to that expected from Primakoff π^o photoproduction.

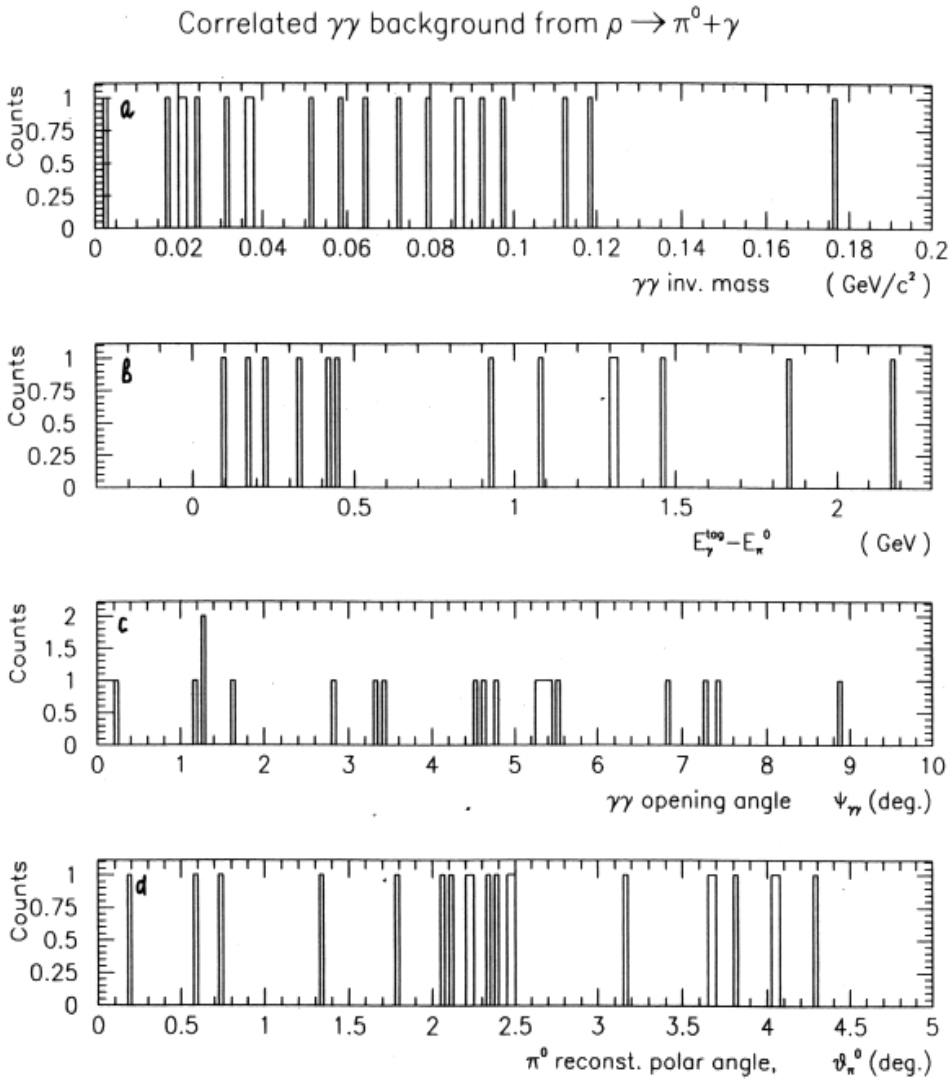

Figure 29: Correlated two photon rates from the rho as a function of (a) invariant mass, (b) missing energy, (c) $\psi_{\gamma 1 \gamma 2}$, and (d) θ_{π^o}. No cuts are applied in the figures.

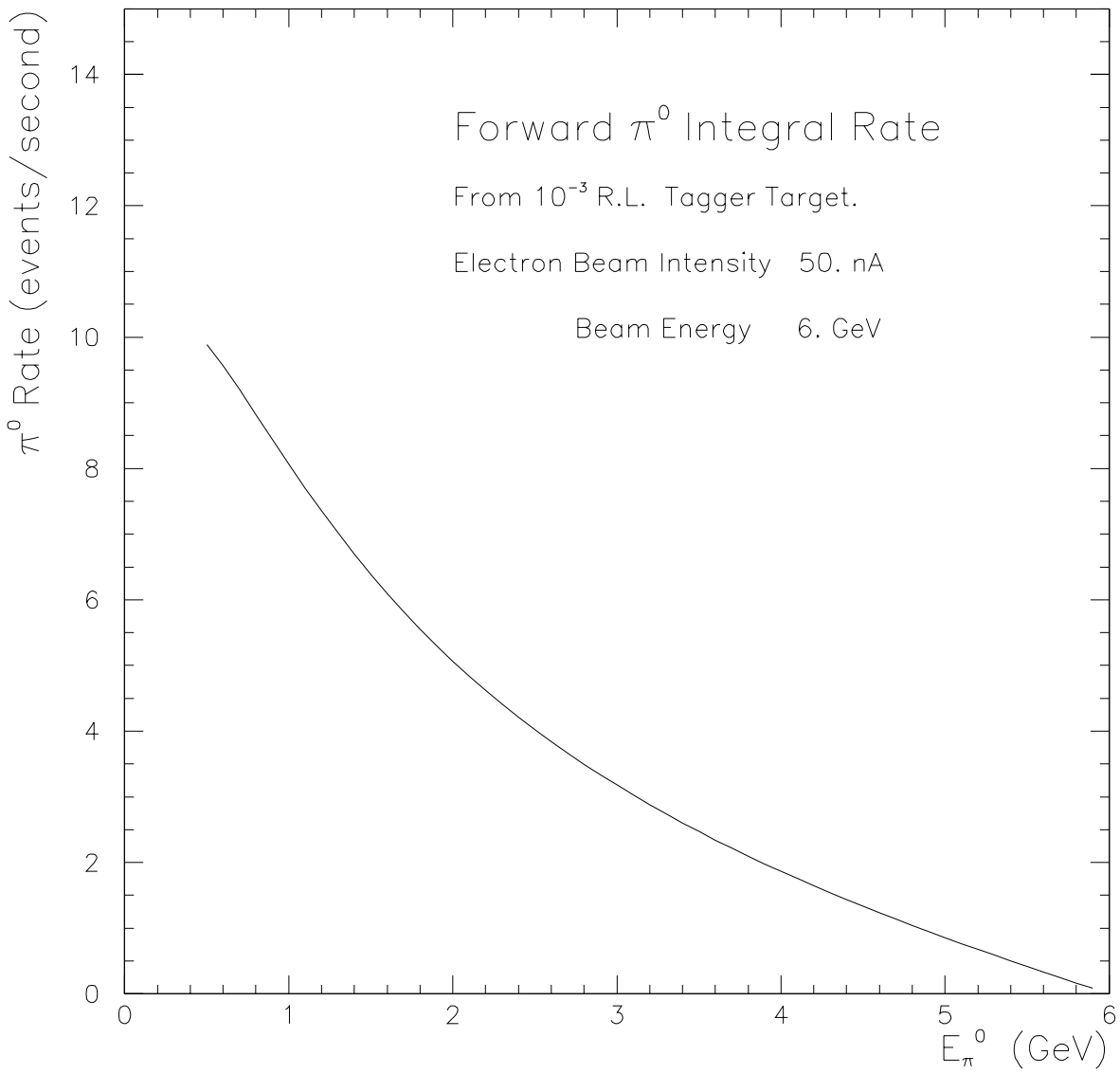

Figure 30: Rate of π^o's produced in the bremsstrahlung converter foil as a function of energy.

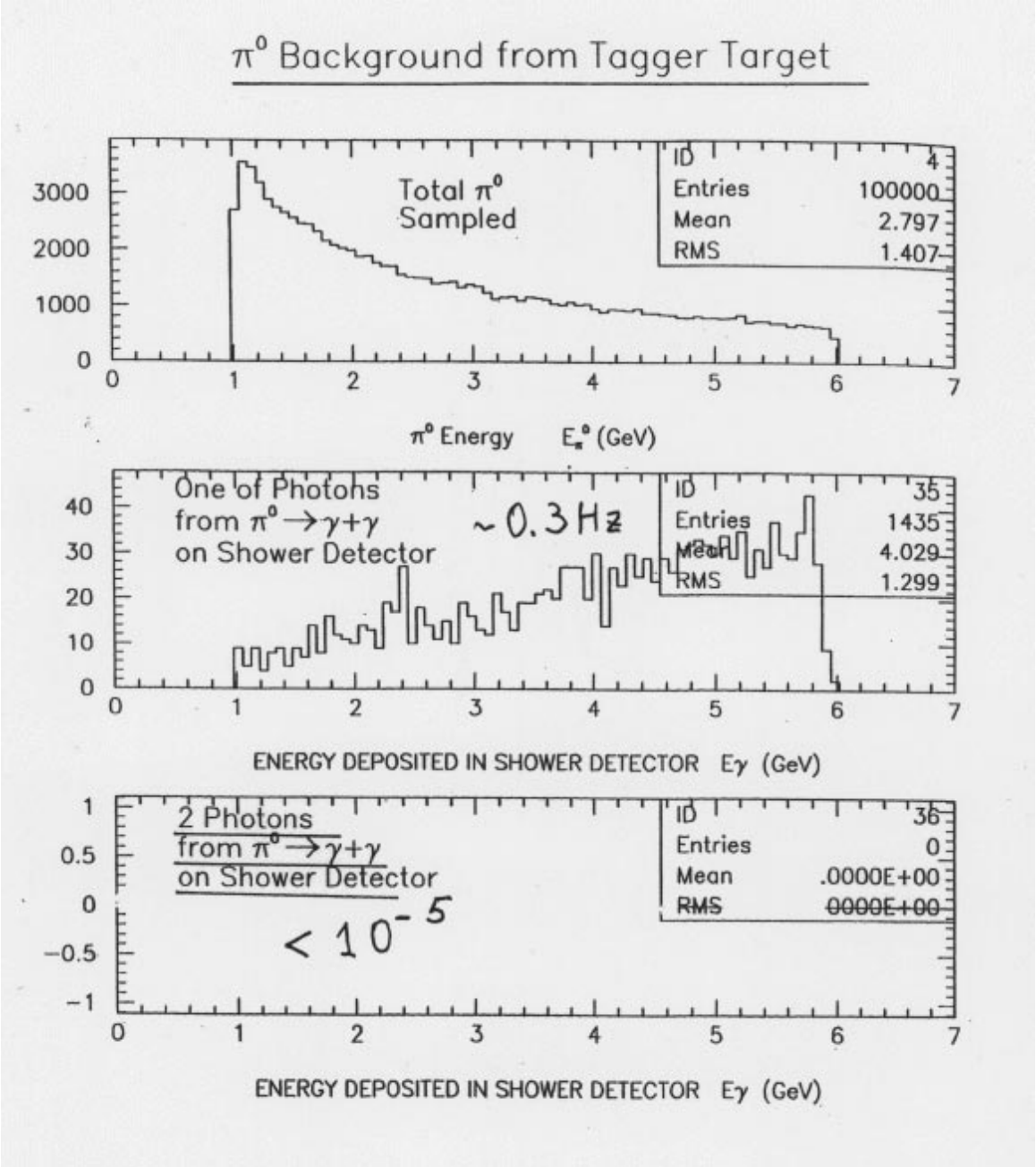

Figure 31: Acceptance of π^o detector to π^o's produced upstream of the Primakoff target. (a), energy distribution of photopions. (b), resulting spectrum of single photon events striking detector. (c) illustrates that the two photon acceptance for these pions is negligible.

spectra if one assumes that the π^o's are produced in the Primakoff production target. When this assumption is correct, *i.e.* the pions are actually produced in the Primakoff target, one obtains the invariant mass distribution indicated in figure 32(a). Those which are produced in the vacuum window or in the iron shielding near the exit of the tagger, however, will give the reconstructed invariant mass spectra indicated in figures 32(b) and 32(c), respectively. While the π^o backgrounds from along the photon beamline are expected to be small, and one can distinguish them on the basis of reconstructed invariant mass, we also plan to directly measure these rates in empty target runs in which the Primakoff production target is removed.

8 Pion final state interactions

The amplitude for coherent photoproduction of pions on nuclei consists of Coulomb and strong components. Each of these are factorized into the amplitude of photoproduction on a nucleon multiplied by a corresponding form factor. The Coulomb form factor which modifies the Primakoff cross section (see equation 3) and the strong form factor which modifies the coherent pion production cross section (see equation 5) must each be corrected for final state interactions of the outgoing pion[41][42]. Since the pions from the Primakoff effect are produced mostly peripherally, the effect of pion final state interactions on the electromagnetic form factor is small. On the other hand, pions produced within the nuclear interior can interact with the nucleus.

The Coulomb form factor is well known and has been calculated in the context of Glauber theory. Using reference [43] as a starting point, we have performed such a calculation for realistic nuclear charge distributions[35], and modified the calculation for the case of π^o photoproduction[44]. The electromagnetic form factor is given by:

$$F_{e.m.} = 2\pi q_t \int b^2 dbdz J_1(q_t b) exp(-\frac{\sigma A}{2} \int_z^\infty \rho(b,z')dz')(b^2+z^2)^{-3/2} \int_0^{\sqrt{(b^2+z^2)}} drr^2\rho(r) \quad (17)$$

where $\rho(x)$ is the charge density, $\vec{q_t}$ is the transverse momentum transfer to the pion, b is the impact parameter, z is the longitudinal coordinate, and σ is the average pion-nucleon total cross section for the outgoing pion. No distinction is made for the charge and matter densities. We have performed the calculation for ^{12}C and ^{208}Pb using realistic three parameter Woods Saxon distributions with parameters taken from [35]. The results of this calculation with and without distortion are shown in figure 33 for ^{12}C and ^{208}Pb.

Figure 34 illustrates the error corridor on the distortion modified Coulomb form factors for (a) ^{12}C, and (b) ^{208}Pb resulting from 10% variation of the measured charge density distributions and pion-nucleon cross section.

The strong form factor is given by:

$$F_N = F_1 + F_2 \quad (18)$$

F_1 is the usual form factor taking into account nuclear absorption. F_2, which was neglected in [41], describes the effect of rescattering of photopions. This is of particular interest in

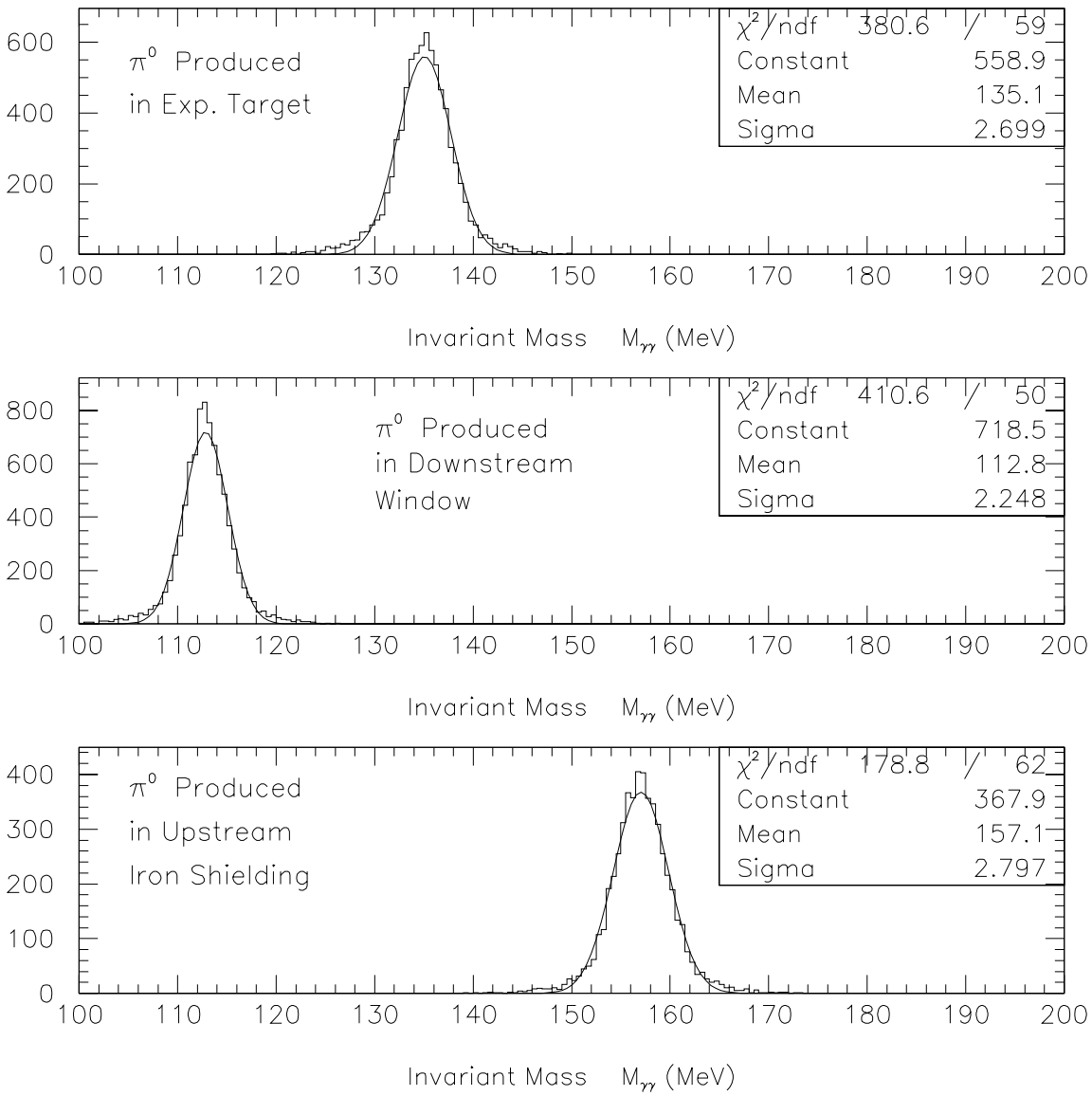

Figure 32: Reconstructed invariant mass distributions for (top), π^o's produced in the Primakoff target, (middle) in the vacuum window between the Primakoff target and the π^o detector, and (bottom) those produced in the iron shielding near the exit of the tagger magnet.

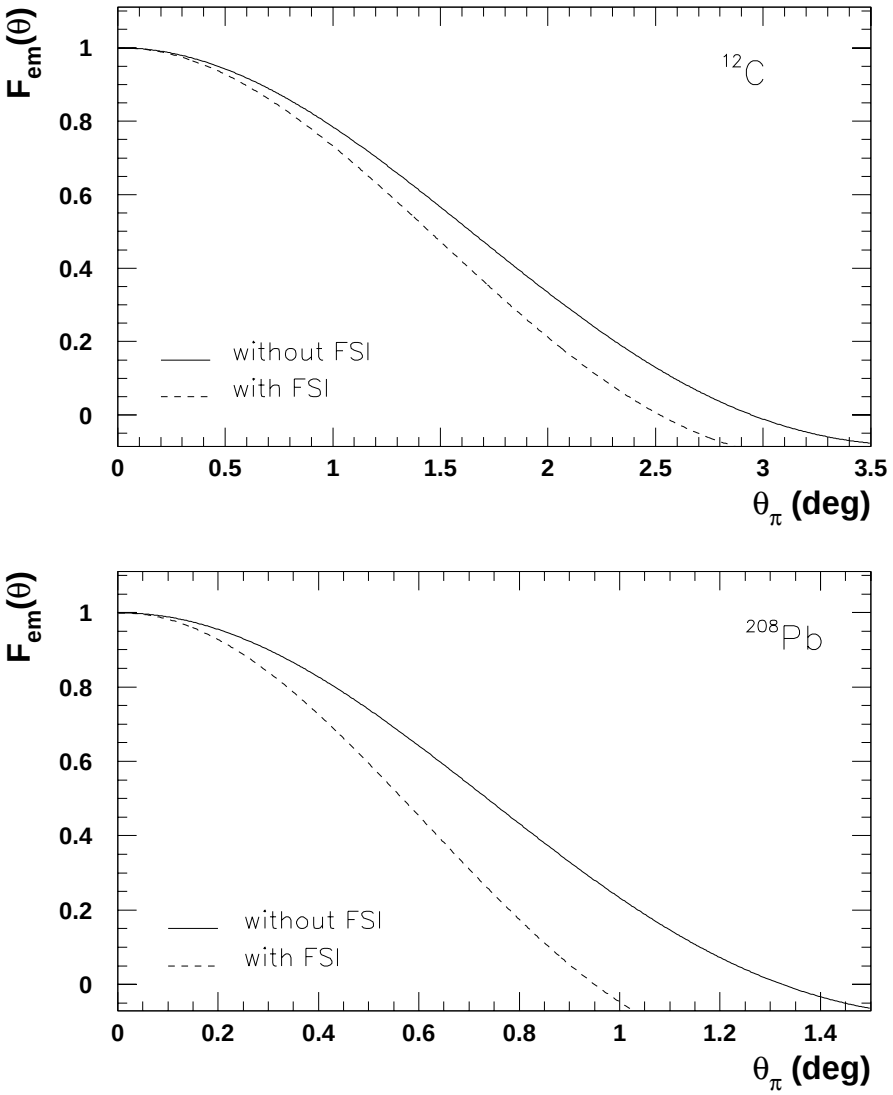

Figure 33: Coulomb form factor with and without distortion for (a) ^{12}C, and (b)^{208}Pb.

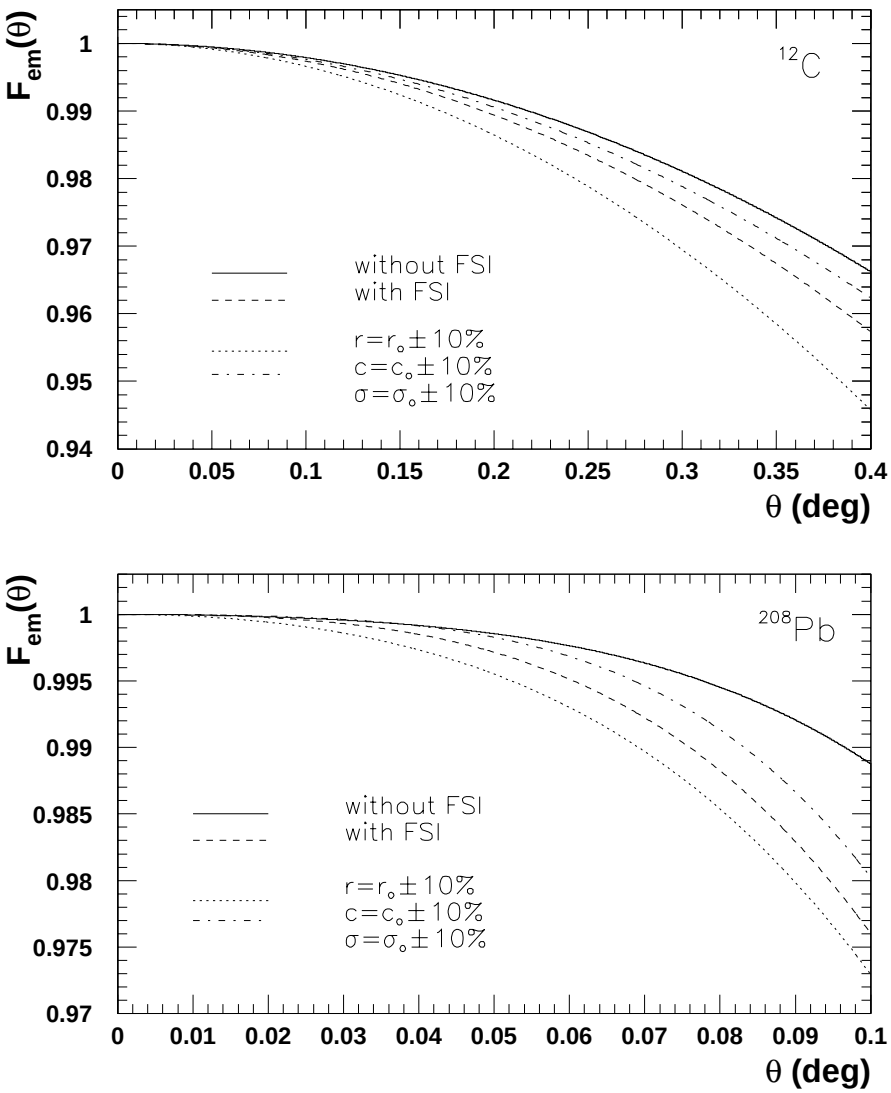

Figure 34: Effect of uncertainties in the Coulomb form factor with distortion due to uncertainties in charge density distributions for (a) ^{12}C, and (b)^{208}Pb.

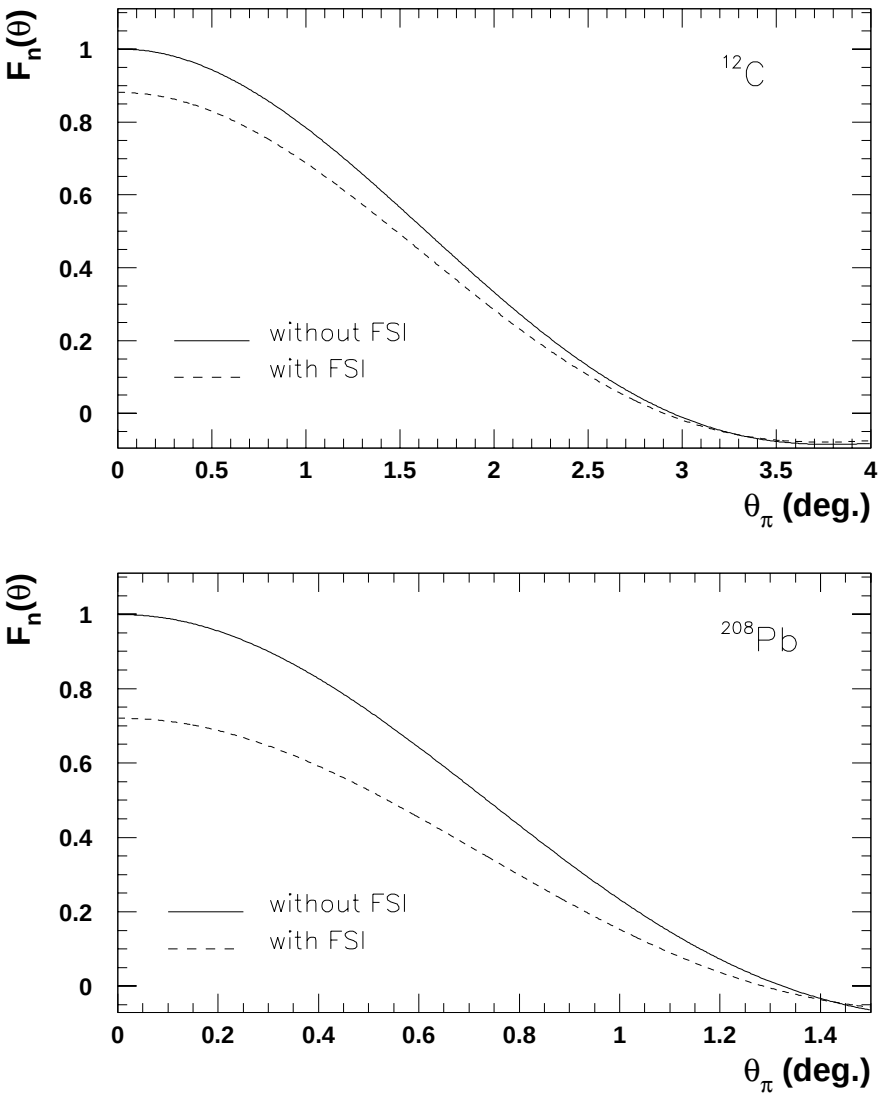

Figure 35: Strong form factor with and without distortion for (a) ^{12}C, and (b)^{208}Pb.

the present experiment since pions produced at modest angles can, as a result of final state interactions, rescatter to small angles under the Primakoff peak. F_1 is given by[44]:

$$F_1(q) = \int d^3x e^{i\vec{q}\cdot\vec{x}} \rho(\vec{x}) e^{-A\frac{\sigma'}{2}\int_z^\infty \rho(b,z')dz'} \tag{19}$$

and F_2 is given by:

$$F_2(q) = -\frac{\pi\sigma A}{q_t}\int_0^\infty J_1(q_t b)bdb \int_{-\infty}^\infty \rho(b,z)dz e^{-\frac{A\sigma}{2}\int_z^\infty \rho(b,z')dz'} \int_z^\infty \frac{d\rho(b,z'')}{db}dz'' \tag{20}$$

The results of the strong form factor so obtained are shown in figure 35(a) and 35(b). The significance of this sometimes neglected [41][16] term, F_2, is illustrated in figure 36.

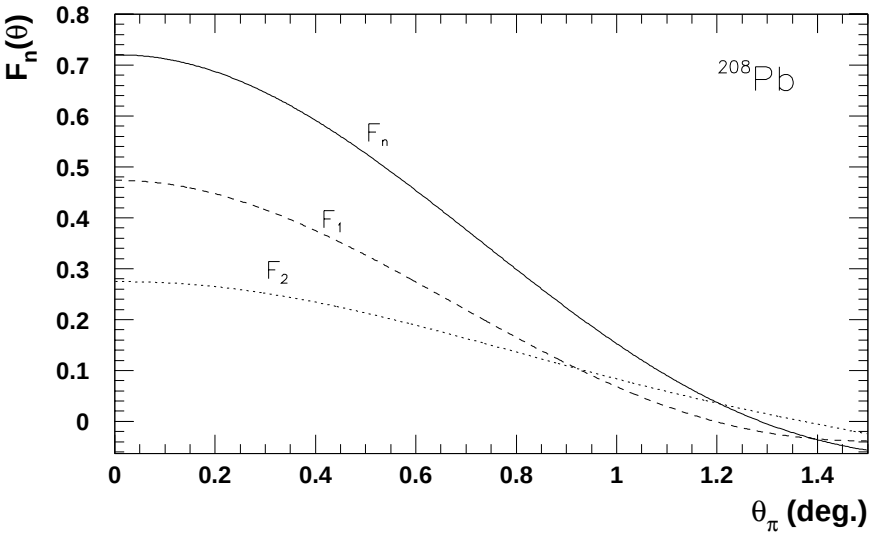

Figure 36: F_1 and F_2 for ^{208}Pb.

9 Experimental uncertainties

We intend to control the experimental errors to make a measurement of the π^o lifetime with a less than 1.5% precision. The various contributions to this error are shown below:

statistical	0.4%
target thickness (atoms/cm^2)	0.7%
photon flux	1.0%
π^o detector acceptance and misalignment	0.4%
background subtraction	0.2%
beam energy	0.2%
distorted form factor calculation errors	0.3%
total	1.4%

The total error was estimated by adding the individual errors in quadrature and represents the expected pion lifetime error from a combined fit of the three Primakoff targets. The errors that are presented are meant to be conservative, *i.e.* we anticipate that we should do no worse than the values given here.

The absolute photon flux will be monitored by measuring the tagging efficiency about once per day. The pair production luminosity monitor will be calibrated against the rates on the tagger at low beam currents and will provide continuous real time relative monitoring throughout the data taking. We will also explore the possibility of making an absolute mea-

surement of the luminosity via pair production in the target using a theoretical calculation of pair production which is expected to be accurate to better than 1%[51].

The targets for this experiment are ^{12}C, ^{116}Sn, and ^{208}Pb, each with thickness 0.05 radiation lengths. The nuclear form factor will be fit to the data at the larger θ_{π^o}'s and therefore its uncertainty will contribute to the statistical error. Errors in the electromagnetic form factor originate from both uncertainties in the nuclear charge distributions and distortion effects. These isotopes were chosen in part because the ground charge densities have been measured in model independent analyses of electron scattering data, and accurate knowledge of the charge density minimizes the uncertainty in the Primakoff vertex due to the charge form factor [45][46][47][48][49][50].

The Sn and Pb targets will be isotopically enriched with purities of 95.7% and 99.9%, respectively. The areal densities (thicknesses) of the ^{12}C, ^{116}Sn, and ^{208}Pb targets are 2135 mg/cm^2 (371 mil), 371 mg/cm^2 (60 mil), and 319 mg/cm^2 (28 mil), respectively.

Oak Ridge has estimated that the uniformity in the Sn and Pb target thicknesses will be at the $\pm 1 - 2\%$ level. For this experiment uncertainties in the target thickness must be kept below the $\pm 0.5\%$ level. Therefore we plan to use oversized targets (2.5 cm $\times$ 2.5 cm) and map target thickness as a function of position on the target. Since the photon beam spot at the target is approximately 2 mm in diameter, the targets can be positioned such that the photon beam strikes a region with known, uniform areal density.

The required accuracy for the ^{12}C target can be achieved using a micrometer with one tenth mil precision, although it is uncertain if the areal density would have the same accuracy due to inhomogeneities in the target density. The use of a micrometer is impossible for the Sn and Pb targets because of the small thickness and softness of the target materials. Therefore we plan to measure the areal densities of the targets by an x-ray absorption method. A source of x-rays is collimated down to a spot size a few mm in diameter and detected in a NaI detector. The Primakoff targets are placed as absorbers between the source and the detector. By measuring the ratio of x-ray flux in the NaI detector for target-in and target-out the areal density of the target can be determined. The method assumes knowledge of the x-ray absorption coefficients, which are typically known at the few percent level. Therefore, at the 1% level this method yields a relative, not absolute, measure of the target density. The relative densities then can be normalized to microscale measurements of the average areal density of the target.

The greatest precision can be obtained by chosing an x-ray energy such that the x-ray absorption length is 1/2 the areal density of the target. This condition determines the optimum x-ray energy to use. For the ^{12}C, ^{116}Sn, and ^{208}Pb targets these energies are approximately 10 keV, 40 keV, and 50 keV, respectively. Therefore the 60 keV x-ray line from ^{241}Am would be appropriate for the Sn and Pb targets. A lower energy x-ray should be used for the carbon measurement. A NaI detector with diameter 2" and thickness 2" is nearly 100% efficient for x-rays at these energies.

The π^o detector acceptance uncertainty arises primarily from edge effects relating to the position resolution in the blocks near the edges of the detector. The edge effects are minimized by excluding the two outermost and innermost layers of lead glass blocks from the fiducial volume. We will control detector offsets to the 0.75 mm level in two ways. First, accurate surveying will fix the π^o detector position with respect to the Hall. Second, position

asymmetries of the photon singles on the detector will be sensitive to offsets with respect to the photon beam and will enable software alignments (see figure 15).

In estimating errors in background subtractions, a 30% uncertainty in calculated background π^o rates was assumed. The effect of the beam energy uncertainty on the extracted lifetime arises from the energy dependence of the Primakoff cross section. With the Hall B tagger, we will be able to control the energy to 1×10^{-3}.

In conclusion, we believe that the error estimates given in the above table are robust. We believe that these or somewhat smaller errors can be achieved. We have discussed the individual ingredients in this section. We also would like to emphasize what was presented in Section 3, namely that the study of the Primakoff peak as a function of Z, photon energy, and pion angle should add a great deal of confidence to the measurement and can be used to empirically determine the systematic errors.

10 Summary

We propose a precision experimental test of the QCD axial anomaly, which is the only essentially parameter free prediction of that theory, with a measurement of the neutral pion two photon decay width. This experiment will reduce the present $\simeq$ 10 % uncertainty to $\simeq$ 1.4% and is arguably one of the most important experiments that can be performed at the present TJNAF energy.

This experiment will use the high intensity, high energy photon tagging facility in Hall B, an array of lead glass detectors with a high resolution, and a $PbWO_4$ crystal insertion, The experiment requires tight control of the systematic errors, mainly connected with the superior π^o detection and knowledge of the absolute value of photon energies and fluxes provided by both the high quality TJNAF electron beam and the photon tagging facility in Hall B.

This proposal is based on one which was submitted to PAC14. In response to concerns raised therein, we have:

- Simulated background rates created in the bremsstrahlung radiator and along the beamline upstream of the Primakoff target.
- Simulated the photon beam profile under the proposed experimental conditions in which the photon collimators are removed. This simulation was cross checked with experimental data.
- Performed state-of-the-art calculations of the effect of pion nucleus final state interactions, including pion rescattering.
- Modified the proposed Primakoff targets to ^{12}C, ^{116}Sn, and ^{208}Pb to test the Z^2 dependence of the extracted Primakoff cross section. Extend the photon range to cover 4.6 to 5.7 GeV to test the E^4 dependence of the Primakoff cross section. The study of the Primakoff peak as a function of Z, E, and pion angle should add a great deal of confidence to the measurement and can be used to empirically determine the systematic errors.
- Provided more detailed simulations of the hybrid lead glass-$PbWO_4$ calorimeter, and have added one additional layer of modules on its outermost boundary. These modules will be excluded from the fiducial volume and will improve control of π^o acceptance. While this detector is expected to suitable for the proposed experiment, construction of a detector comprised entirely of $PbWO_4$ modules, with its concomitant increase in cost, remains an option.

We are requesting 22 days of beam time at 6 GeV, 7 days on carbon and 6 days of data taking each for the ^{116}Sn and Pb targets, and 3 days of empty target and detector calibration runs. Major new equipment for this experiment includes a multichannel hybrid lead glass/$PbWO_4$ π^o detector and a 15 kilogauss·m dipole magnet for use as a sweeping magnet and pair production luminosity monitor.

References

[1] J.S. Bell et al., Il Nuovo Cimento, vol. 51, no. 1., (1969), 47.

[2] S. Adler, Phys. Rev., vol. 177, no. 5, (1969), 2426.

[3] J. Bijnens, A. Bramon and F. Cornet, Phys. Rev. Lett. 61 (1988) 1453.

[4] J.F. Donoghue, B.R Holstein, Y.C.R. Lin, Phys. Rev. Lett., vol. 55, no. 25, (1985), 2766; J.F. Donoghue, B. Wyler, Nuc. Phys., B316, (1989), 289.

[5] J. Bijnens et al., Z. Phys. C, 46, (1990), 599.

[6] J. Bijens, J. Prades, Z. Phys. C64, (1994), 475.

[7] A.M. Bernstein, Nuc. Phys. A623 (1997) 178c..

[8] R.M. Barnett et al., Review of Particle Physics, Phys. Rev., D54, (1996), 21.

[9] See, *e.g.* Dynamics of the Standard Model, J.F. Donoghue, E. Golowich, and B.R. Holstein, Cambridge University Press (1992).

[10] D. Dale, A. Gasparian, Proposal to TJNAF PAC12, E-97-009, (1997).

[11] G. von Darder et al., Phys. Lett., vol. 4, no. 1, (1963), 51.

[12] H.W. Atherton et al., Phys. Lett., vol. 158B, no. 1, (1985), 81.

[13] D.A. Williams et al., Phys. Rev. D, vol. 38, no. 5, (1988), 1365.

[14] H. Primakoff, Phys. Rev. 81, 899 (1951).

[15] A. Browman et al., Phys. Rev. Letts., vol. 33, no. 23, (1974), 1400.

[16] G. Bellettini et al., Il Nuovo Cimento, vol. 66, no. 1, (1970), 243.

[17] V.I. Kryshkin et al., Sov. Phys. JETP, vol. 30, no. 6, (1970), 1037.

[18] G. Bellettini et al., Il Nuova Cimento, vol. 40, no. 4, (1965), 1139.

[19] D.I. Sober, A Guide to the Optics of the Tagged Photon Magnet, CLAS Note 91-012.

[20] J. Arends, M. Breuer, H.D. Dahmen, P. Detemple, W. Schneider, D. Urban and B. Zucht, NIM A306 (1991), 89.

[21] G.A. Alexeev, *et al.*, NIM A364, (1995), 307.

[22] H. Stroher, G. Koch, V. Metag, R. Beck, B. Schoch, J. Vogt, NIM A269 (1988), 568.

[23] Proposal for a High Resolution Spectrometer for Neutral Mesons, Los Alamos National Laboratory, December 1989.

[24] B. Powel et al., Nucl. Instr. and Meth., 198, (1982), 217.

[25] A.S. Aleksanian et al., Preprint YerFI-1239-25-90, (1990).

[26] D.I. Sober, private communication.

[27] T.J. Brodbeck, P. Coddington, J.V. Morris, D. Newton, T. Sloan, Nucl. Phys B136 (1978) 95.

[28] J. Ballam, G.B. Chadwick, Z.G.T. Guiragossian, A. Levy, M. Menke, P. Seyboth, G. Wolf, Phys. Lett., vol. 30B, no. 6 (1969) 421.

[29] Y. Eisenberg, B. Haber, Carmel, E. Peleg, E.E. Ronat, A. Shapira, G. Vishinsky, R. Yaari, G. Yekutirli, Phys. Rev. Lett., vol. 22, no 13 (1969) 669.

[30] Y. Eisenberg, B. Haber, E.E. Ronat, Y. Stahl, G. Yekutirli, J. Ballam, G.B. Chadwick, M.M. Menke, P. Seyboth, A. Shapira, J. Gandsman, J. Grunhaus, A. Levy, Phys. Lett, vol. 34B, no. 5 (1971) 439.

[31] D.O. Caldwell, V.B. Elings, W.P. Hesse, R.J. Morrison, F.V. Murphy, Phys. Rev. D, vol. 7, no. 5 (1973) 1362.

[32] T.H. Bauer, R.D. Spital, D.R. Yennie, Rev. Mod. Phys., vol. 50, no. 2 (1978) 261.

[33] P.L. Braccini, C. Bradaschia, R. Castaldi, L. Foa, K. Lubelsmeyer, D. Schmitz, Nucl. Phys. B24 (1970) 173.

[34] H.-J. Behrend, F. Lobkowicz, E.H. Thorndike, A.A. Wehmann, Phys. Rev. Lett., vol 24, no. 22 (1970) 1246.

[35] de Jager, de Vries, deVries, At. Data and Nuc. Data Tables, vol. 14, no. 5 (1974) 480.

[36] J.B. Bellicard and K.J. van Oostrum,Phys. Rev. Lett., vol. 19, no. 5, (1969) 242.

[37] G.J.C. van Niftrik, Nuc. Phys. A131, (1969), 574.

[38] J. Heisenberg, R. Hofstader, J.S. McCarthy, I. Sick, B.C. Clark, R. Herman, D.G Ravenhall, Phys. Rev. Lett., vol. 23, no. 24. (1969),1402.

[39] J. Friedrich, F. Lenz, Nuc. Phys. A183 (1972), 523.

[40] H. Euteneuer, J. Friedrich, N. Voegler, Phys. Rev. Lett., vol. 36, no. 3, (1976) 129.

[41] G. Morpurgo, Nuovo Cimento, 31, (1964), 569.

[42] C.A. Engelbrecht, Phys. Rev. 133, (1964), 988.

[43] G. Faldt, Nucl. Phys. B43, (1972),591.

[44] S. Gevorgyan, private communication.

[45] L.S. Cardman et al., Phys. Lett. 91B, 203 (1980).

[46] W. Reuter, et. al., Phys. Rev. C26, 806 (1982).

[47] I. Sick, Phys. Lett. 116B, 212 (1982) .

[48] J.M. Cavedon, et. al., Phys. Lett. 118B, 311 (1982) .

[49] B. Frois, et. al., Phys. Rev. Lett. 38, 152 (1977).

[50] H. Euteneuer, et. al., Nucl.Phys. A298, 452 (1978)).

[51] L. Maximon, private communication.